Elisabeth Woisetschläger, BSc

Combined estimation of geocenter motion from GRACE gravimetry and IGS station loading deformation

MASTERARBEIT

zur Erlangung des akademischen Grades
Diplom-Ingenieurin

Masterstudium Geomatics Science

Technische Universität Graz

Betreuer:

Univ.-Prof. Dr.-Ing. Torsten Mayer-Gürr

Institut für Theoretische Geodäsie und Satellitengeodäsie

Graz, September 2014

“If we knew what it was we were doing, it would not be called research, would it?“

Albert Einstein

Abstract

As the Earth is a dynamic system, masses (surface loads) are redistributed on the Earth's surface. This redistribution is causing a motion of the center of mass of the solid Earth (CE) in inertial space. In contrast, the center of mass of the Earth system (CM), which includes the solid Earth and the surface load, does not relocate due to surface loading. The difference between the CE and the CM is defined as "geocenter motion" in this thesis.
Load induced deformations of the Earth's crust can be observed by GPS stations. As the GPS sites of the International GNSS Service (IGS) are globally distributed, their load induced deformation observations are used to calculate the geocenter motion. More precisely, the load potential coefficients are estimated with the help of these observations. The degree-1 potential coefficients are defining the center of mass and are therefore reference frame dependent. Consequently, the geocenter motion can be directly linked to degree-1 surface loading coefficients.
Furthermore, load potential coefficients derived from GRACE (Gravity Recovery And Climate Experiment) observations were used in an combined least squares adjustment with the GPS data. As GRACE satellites are orbiting the CM, degree-1 potential coefficients cannot be directly calculated. However, when using GRACE data lower degree coefficients can be better separated and the geocenter motion can be calculated more precisely. Additionally, seven Helmert transformation parameters were estimated together with the loading potential coefficients and represent deformation movements not caused by surface loading.

Kurzfassung

Die Erde ist ein dynamisches System, wodurch es zu Verlagerungen von Massen (Auflasten) auf der Erdoberfläche kommt. Wenn dies nun im Interatialsystem betrachtet wird, verursachen diese Massenverlagerungen eine Bewegung des Massenzentrums der festen Erde (CE). Jedoch verursachen sie keine Änderung des Massenzentrums des Erdsystems (CM), da das Erdsystem die feste Erde sowie die Oberflächenauflasten beinhaltet. Die Differenz des CE und des CM wird in dieser Arbeit als "Geozentrumsbewegung"bezeichnet.
Deformationen der Erdkruste, verursacht durch Auflasten, können mit Hilfe von GPS-Stationen beobachtet werden. Da GPS-Stationen des Internationalen GNSS Services (IGS) weltweit verteilt sind, wurden deren Beobachtungsdaten zur Berechnung der Geozentrumsbewegung herangezogen. Genau genommen wurden mit diesen Beobachtungen Auflast-Potentialkoeffizienten geschätzt. Da die Grad-1 Potentialkoeffizienten das Massenzentrum definieren und daher abhängig vom Referenzrahmen sind, kann die Geozentrumsbewegung direkt mit diesen in Verbindung gebracht werden.
Darüber hinaus wurden Auflast-Potentialkoeffizienten, abgeleitet aus GRACE (Gravity Recovery And Climate Experiment) Beobachtungen, einem Ausgleich mit GPS-Beobachtungen hinzugeführt. Da GRACE-Satelliten das CM umkreisen, können die Grad-1 Potentialkoeffizienten nicht direkt aus GRACE-Beobachtungen abgeleitet werden. Jedoch können durch das Hinzufügen von GRACE-Daten Koeffizienten mit niedrigen Grad besser separiert und somit die Geozentrumsbewegung genauer berechnet werden. Ebenso wurden sieben Helmert-Transformationsparameter gleichzeitig mit den Auflast-Potentialkoeffizienten geschätzt. Diese repräsentieren Deformationsbewegungen, welche nicht durch Auflast verursacht wurden.

Acknowledgements

Herewith, I would like to thank my supervisor Prof. Torsten Mayer-Gürr for his guidance and support during this thesis. He was always willing to lend a sympathetic ear and made it possible for me to explore a current issue of research in the course of the last year. Not only his expertise but also the friendly atmosphere at the institute have simplified the completion of this thesis.

I also want to express particular gratitude to my parents, who have not only supported me financially but have also been important mentors throughout my entire education.
Furthermore, I would like to thank my dear friend Barbara for proofreading my thesis and for being a loving friend overall. I also want to accentuate my boyfriend's support and encouragement throughout this thesis; without him I would have found myself in despair much more often. Finally, I would like to thank my friends and colleges, who have made my years as a university student very special.

EIDESSTATTLICHE ERKLÄRUNG
AFFIDAVIT

Ich erkläre an Eides statt, dass ich die vorliegende Arbeit selbstständig verfasst, andere, als die angegebenen Quellen/Hilfsmittel nicht benutzt, und die den benutzen Quellen wörtlich und inhaltlich entnommenen Stellen als solche kenntlich gemacht habe. Das in TUGRAZonline hochgeladene Textdokument ist mit der vorliegenden Masterarbeit identisch.

I declare that I have authored this thesis independently, that I have not used other than the declared sources/resources, and that I have explicitly indicated all material which has been quoted either literally or by content from the sources used. The text document uploaded to TUGRAZonline is identical to the present master's thesis.

Datum/*Date*	Unterschrift/*Signature*

Contents

1 Introduction

The objective of this thesis is to calculate the geocenter motion, the offset between the Center of Mass of the solid Earth (CE) and the Center of Mass of the Earth System (CM).
As the Earth is a dynamic system, masses (surface loads) are redistributed on the Earth's surface. These temporal variations are caused by e.g. the hydrologic cycle. Due to those redistributions the CE changes its position in inertial space. As the Earth System is defined as the solid Earth plus the surface load, the CM does not move due to loading in inertial space. The CE frame is suitable to describe the dynamics of the solid Earth. However, the CE cannot be directly observed. Fortunately, the Center of Network (CN) approaches the CE well when using globally evenly distributed stations. As IGS GPS stations cover most parts of the Earth, their observations were used to calculate the geocenter motion.
Temporal variations of the Earth's system are not only caused by loading but also by influences of the Earth's mantle and crust (plate tectonics). Those variations are represented by a trend or a jump (earthquake) in the time series. As a load induced geocenter motion has to be calculated, those effects have to be eliminated from the time series. This is accomplished in this theses with a jump detection and a subsequent trend elimination.
Loading potential coefficients are estimated with the jump eliminated and detrended GPS time series. As the degree-1 potential coefficients define the center of mass and consequently the reference system, those coefficients are then used to calculate the geocenter motion. Therefore, the geocenter motion can be directly linked to the degree-1 loading potential coefficients. The geocenter motion can be calculated by using degree-1 load Love numbers to transform the CE frame into the CM frame. Those load Love numbers describe the deformation of the Earth's surface due to loading.
Additionally, potential coefficients derived from GRACE (Gravity Recovery And Climate Experiment) observations are used for calculations. As GRACE satellites orbit the CM, only coefficients of degrees higher than one can be computed. Thus, the GRACE input data does not directly influencing the result of the geocenter motion. However, when adding GRACE data to a combined least squares adjustment, loading potential coefficients of lower degrees can be better separated and the result of the geocenter motion becomes more accurate.
Furthermore, seven Helmert transformation parameters t_x, t_y, t_z (translation), s (scale) and r_x, r_y, r_z (rotation) are estimated together with the loading potential coefficients. Those parameters represent deformation movements not caused by surface loading.

Although the geocenter motion is in the range of a few millimeters, it is important for different geodetic applications. For instance, the interpretation and appliance of the ITRF (International Terrestrial Reference Frame) is one of many examples [Wu et al., 2012].

2 Theoretical background

In this chapter, the theoretical background of this thesis is discussed. As GRACE and GPS Satellite data are used in this work, those two satellite missions are described at the beginning. Furthermore, the potential theory, the dynamic Earth system as well as the frame theory are discussed.

2.1 Satellite Missions

2.1.1 GRACE - Gravity Recovery And Climate Experiment

The "Gravity Recovery And Climate Experiment" (GRACE) gravity field satellite mission was launched in 2002. It is a joint mission of NASA *(National Aeronautics and Space Administration)* and DLR *(Deutsches Zentrum für Luft- und Raumfahrt)* [Tapley et al., 2004].

GRACE has two identical satellites (twin satellites) orbiting the Earth in a polar orbit (inclination of 89°) and at an altitude of 470 kilometers. The distance between the satellites amounts to 220 kilometers (see Fig. 1). Due to the low altitude, the satellites' time of circulation around the Earth is 94 minutes. A global coverage is available after 30 days.
Due to GRACE's high-accuracy measurements, it is possible to determine temporal variation of the Earth's gravity field (see chapter 2.3.1). Usually, those temporal variations are given in monthly time series. However, in this thesis, daily gravity field solutions were used [Kurtenbach, 2011].

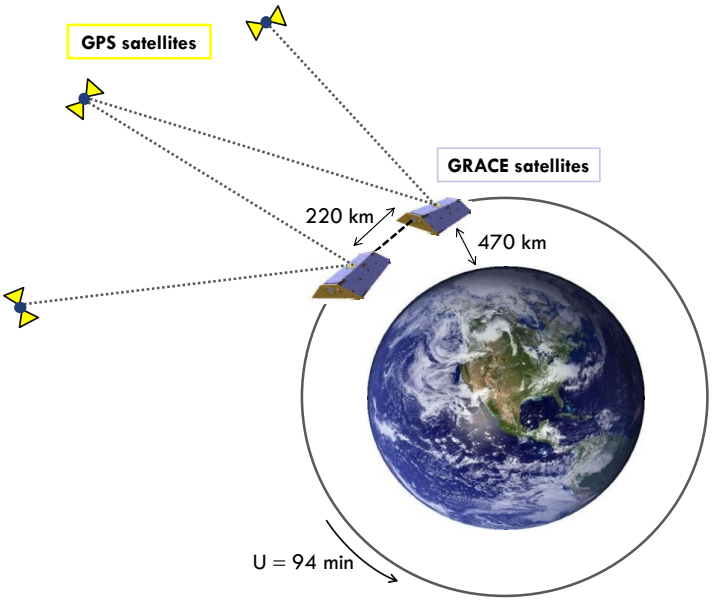

Figure 1: Schematic diagram illustrating the GRACE mission

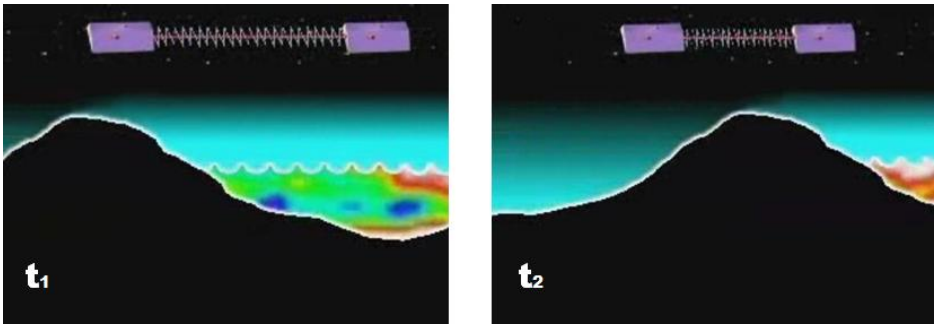

Figure 2: GRACE satellites flying over a landmass [University of Texas, 2014]

The payload of GRACE satellites mainly consists of a K-band ranging system, a GPS space receiver, an accelerometer, a laser retro reflector as well as a Star Camera Assembly [GFZ, 2014; Kurtenbach, 2011].

K-band ranging system. The Earth's gravity field is location-dependent. Because of this and the fact that the GRACE twin satellites fly apart from each other, those gravitational changes attract the spacecrafts differently. Due to this, the distance between the satellites changes (see Fig. 2). This varying distance is measured by the K-band ranging system with an accuracy better than $1\,\mu m/s$. Consequently, the relative position of the satellites to each other can be determined. This measurement method is called *"low-low satellite to satellite tracking" (low-low SST).*

Accelerometer. All non-gravitational accelerations, due to e.g. air drag or solar radiation pressure, are measured by the accelerometer. Those accelerations also cause a change in the satellite's orbit and consequently have to be considered before deducing the Earth's gravity field. The accelerometer's measurement accuracy is $3 \cdot 10^{-10} \frac{m}{s^2}$.

GPS space receiver. The absolute position of the GRACE satellites is determined with the help of GPS measurements. This can be done with an accuracy of two to three centimeters. This measurement concept is called *"high-low satellite to satellite tracking" (high-low SST).* Furthermore, with GPS all payload data can be tagged with a time stamp and an atmospheric and ionospheric profiling can be performed.

Laser retro reflector. The laser retro reflector is a simple passive payload instrument, which reflects short laser pulses of visible and near-infrared wavelength. In combination with GPS, the reflector's data is used to determine a precise orbit and to calibrate the on-board GPS space receiver.

Star camera assembly. The star camera assembly serves for determining the orientation of the satellite with respect to the stars as well as for correctly interpreting the accelerometer measurements.

2.1.2 GPS - Global Positioning System

The Global Positioning System (GPS) is one of the global navigation satellite systems (GNSS) and therefore enables positioning anytime and anywhere on Earth with the help of satellites. It was developed in the 1970s by the US Department of Defense (DOD) and was fully functional in 1995. Nominally, 24 GPS satellites orbit the Earth at an altitude of 20 200 km. Those satellites are arranged on six planes, which have an inclination of approximately 55°. The orbital period amounts to approximately 12 hours and the ground track repeat period to one sidereal day.
The GPS satellites transmit signals, which are collected by GPS receivers on Earth. The basic concept of GNSS is based on the traveling time of the signal between the satellite and the receiver. This time difference multiplied with the speed of light results in the apparent range between the satellite and the receiver/user. As the position of the satellite is estimated by operations centers, the user's position can be calculated. However, in practice influences as receiver and satellite clock errors as well as ionosphere and troposphere based errors have to be considered. For more details see Hofmann-Wellenhof et al. (2008).

IGS Station Network. The International GNSS Service (IGS) was established by the International Association of Geodesy (IAG) in the early 1990s. With the help of a tracking network of more than 400 (status as of 2014) globally distributed tracking sites (see Fig. 3), the IGS provides high quality GNSS data products. Among other things, those products include GNSS satellite orbit data, global tracking station coordinates and velocities as well as global ionospheric maps. The products are available in different time spans and are transmitted in software independent exchange formats. Products with a low accuracy are available in (near) real-time. The final products with the highest accuracy are available after approximately two weeks. [Hofmann-Wellenhof et al., 2008; IGS, 2014].
As the IGS network consists of globally distributed tracking sites with high quality coordinate information, the displacement data of those stations is used in this thesis.

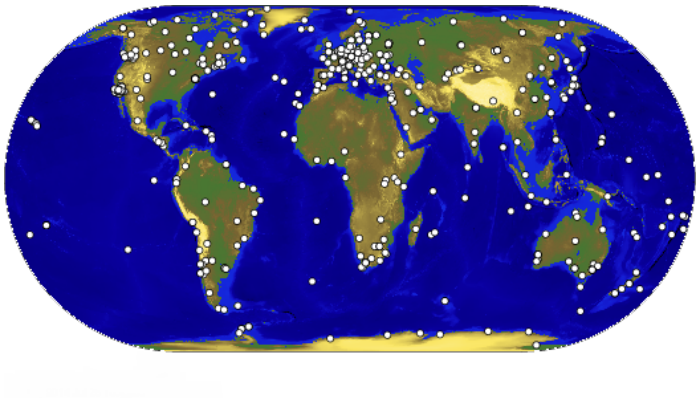

Figure 3: IGS tracking network (sites displayed with white dots) [IGS, 2014]

2.2 Fundamentals of potential theory

Gravitational potential. As described in Moritz et al. (2006) the gravitational potential of a solid body can be described by Newton's integral

$$V(x,y,z) = G \iiint_{\nu} \frac{\rho}{l}\,\mathrm{d}\nu = G \int_{\xi}\int_{\eta}\int_{\zeta} \frac{\rho(\xi,\eta,\zeta)}{\sqrt{(x-\xi)^2+(y-\eta)^2+(z-\zeta)^2}}\,\mathrm{d}\xi\,\mathrm{d}\eta\,\mathrm{d}\zeta\,. \qquad (1)$$

With this equation, the potential of an attracted point $P(x,y,z)$ can be calculated under consideration of all mass elements $dm(\xi,\eta,\theta)$ in a volume v and their local density ρ (see Fig. 4). The variable l stands for the distance between the attracted point P and the mass element dm. The gravitational constant G has the value $6.67384 \cdot 10^{-11} \frac{m^3}{kg \cdot s^2}$.

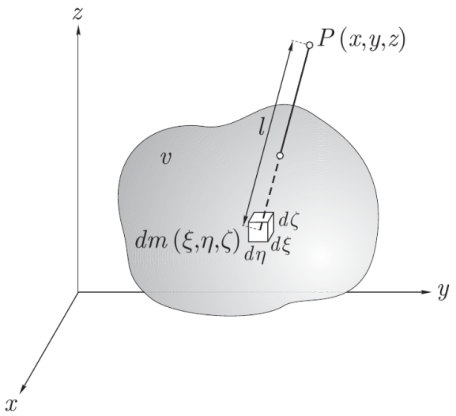

Figure 4: Schematic drawing of the potential of a solid body [Moritz et al., 2006]

Spherical harmonics expansion. The gravitational potential can be expressed in terms of a spherical harmonics expansion. The spherical harmonics expansion for the Earth's exterior, which was used for calculations in this thesis, can be displayed as follows:

$$V(r,\lambda,\vartheta) = \frac{GM}{R} \sum_{n=0}^{\infty} \left(\frac{R}{r}\right)^{(n+1)} \sum_{m=0}^{n} c_{nm}\, C_{nm}(\lambda,\vartheta) + s_{nm}\, S_{nm}(\lambda,\vartheta)\,. \qquad (2)$$

In equation (2), the attracted point is, in contrast to equation (1), described by spherical coordinates r, λ, φ. The geocentric gravitational constant GM is the product of the gravity constant G and the Earth's total mass M. It is divided by the Earth's radius R. The degree n

and order m dependent potential coefficients c_{nm} and s_{nm} are multiplied with the basis functions $C_{nm}(\lambda, \vartheta)$ and $S_{nm}(\lambda, \vartheta)$. Those basis functions are displayed in equation (3) and consist of the fully normalized Legendre polynomial P_{nm} and a sine and cosine term respectively [Moritz et al., 2006]

$$\begin{aligned} C_{nm}(\lambda, \vartheta) &= P_{nm}(\cos\vartheta)\, \cos(m\lambda) \\ S_{nm}(\lambda, \vartheta) &= P_{nm}(\cos\vartheta)\, \sin(m\lambda)\,. \end{aligned} \tag{3}$$

Center of mass. The potential coefficients c_{nm} and s_{nm} can be physically interpreted [Moritz et al., 2006]. After equating the coefficients of equations (1) and (2), these potential coefficients can be expressed as follows:

$$\begin{Bmatrix} c_{nm} \\ s_{nm} \end{Bmatrix} = \frac{1}{M(2n+1)} \iiint_{\Omega} \left(\frac{r'}{R}\right)^n \begin{Bmatrix} C_{nm}(\lambda', \vartheta') \\ S_{nm}(\lambda', \vartheta') \end{Bmatrix} \rho(\mathbf{r}')\, d\Omega\,. \tag{4}$$

It has to be mentioned that the spherical coordinates λ', ϑ' and r' in equation (4) describe the position of the attracting point. Inserting the basis functions $C_{nm}(\lambda, \vartheta)$ and $S_{nm}(\lambda, \vartheta)$ of degree-1

$$\begin{aligned} C_{10}(\lambda, \vartheta) &= \sqrt{3}\cos\vartheta = \sqrt{3}\frac{z}{r} \\ C_{11}(\lambda, \vartheta) &= \sqrt{3}\sin\lambda\sin\vartheta = \sqrt{3}\frac{x}{r} \\ S_{11}(\lambda, \vartheta) &= \sqrt{3}\cos\lambda\sin\vartheta = \sqrt{3}\frac{y}{r} \end{aligned} \tag{5}$$

in equation (4) as well as under consideration of the definition of the center of mass

$$\mathbf{r}_0 = \begin{pmatrix} x_0 \\ y_0 \\ z_0 \end{pmatrix} = \frac{1}{M} \iiint_{\Omega} \mathbf{r}'\, \rho(\mathbf{r}')\, d\Omega\,, \tag{6}$$

the potential coefficients of degree-1 can be calculated as follows:

$$\begin{aligned} c_{10} &= \frac{\sqrt{3}}{3R}\, z_0 \\ c_{11} &= \frac{\sqrt{3}}{3R}\, x_0 \\ s_{11} &= \frac{\sqrt{3}}{3R}\, y_0\,. \end{aligned} \tag{7}$$

Therefore, the choice of degree-1 potential coefficients defines the center of mass and thus the reference system.

2.3 The dynamic Earth system

The Earth is a dynamic system, which processes cause temporal variations of the Earth's gravity field. Those effects as well as calculations of the potential of temporal variations are described in this chapter.

2.3.1 Temporal variations of the Earth's gravity field

Due to GRACE data, information about temporal variations of the Earth's gravity field can be provided globally. Processes responsible for those temporal variations are shown in table 1. As displayed in this table, the effect on the Earth's figure (given in geoid height differences ΔN) as well as the spacial extent varies from process to process. Moreover, it can be inferred from table 1 that the sources of temporal variations of the Earth's gravity field are occurring in different time intervals.
The listed processes can be divided into four main groups: *"Solid Earth and ocean tides"*, *"Hydrologic cycle"*, *"Ice mass variations"* and *"Secular processes of the Earth's interior"* [Kurtenbach, 2011].

Solid Earth and ocean tides. The solid Earth and ocean tides, caused by the gravity of Moon and Sun, have the biggest influence on temporal variations of the Earth's gravity field. This can be seen in table 1, as the effect on the geoid height is in the range of a few decimeters. The effect of the solid Earth and ocean tides is well estimated by models and is therefore reduced during GRACE and GPS data processing.

Hydrologic cycle. The Earth's hydrologic cycle consists of many processes, e.g. condensation, precipitation or evaporation. The effect of the hydrologic cycle as well as its processes on the Earth's gravity field can be mainly divided into influences of the atmosphere, of ocean currents and of continental hydrology. Those influences have an impact of a few centimeters on the geoid height and a varying temporal occurrence due to different climatic effects.

Ice mass variations. The Geoid is seasonally deforming within the range of a few millimeters due to snow melt and snow accumulation. Furthermore, multi-annual ice-mass loss secularly changes the Earth's gravity field.

Secular processes of the Earth's interior. Secular processes changing the Earth's gravity field are divided into effects of the Earth's mantle and crust as well as into the influence of the post-glacial rebound. The change of the geoid height is in the order of a few millimeters per year. Processes of the Earth's mantle and crust are not only continuous long-term plate motions but also instantaneous mass changes due to e.g. earth quakes.
At this point it has to be mentioned, that the influences of the Earth's mantle and crust were removed in this thesis by means of a trend elimination and a jump detection (see chapter 3). Unfortunately, the effect of post-glacial rebound is mainly linear and thus mostly eliminated by those processing methods.

Therefore, only temporal variations of the Earth's gravity field caused by seasonal ice mass variations and effects of the hydrologic cycle influence the results.

Table 1: Sources of temporal variations of the Earth's gravity field [Kurtenbach, 2011]

Process	**Spatial extent** [km]	**Temporal occurrence**	**Effect** [ΔN]
Solid Earth and ocean tides	10 to 10000	daily, semi-daily, monthly	dm
Atmosphere	50 to 5000	yearly, seasonal, daily and others	cm
Ocean currents	30 to 5000	seasonal to yearly, secular	cm
Continental hydrology	100 to 5000	daily, weekly to yearly	cm
Cryosphere	100 to 4000	seasonal to multi-annual	mm
Post-glacial rebound	500 to 10000	secular	mm/year
Earth's mantle and crust	100 to 2000	secular	mm/year

2.3.2 Surface loading

As the Earth is a dynamic system, masses are redistributed and therefore the Earth's gravity field shows temporal variations. These global variations can be measured with GRACE and can be described with a potential, called the total potential V^{total}. This total potential can be divided into the loading potential V^{load} and the deformation potential V^{defo}

$$V^{total} = V^{load} + V^{defo}\,. \tag{8}$$

The loading potential V^{load} describes the direct effect on the Earth's gravity field caused by mass redistribution. It can be expressed by a spherical harmonics expansion at the Earth's surface

$$V^{load}(r,\lambda,\vartheta) = \frac{GM}{R}\sum_{n=0}^{\infty}\sum_{m=0}^{n} P_{nm}(\cos\vartheta)[c_{nm}\,\cos(m\lambda) + s_{nm}\,\sin(m\lambda)]\,. \tag{9}$$

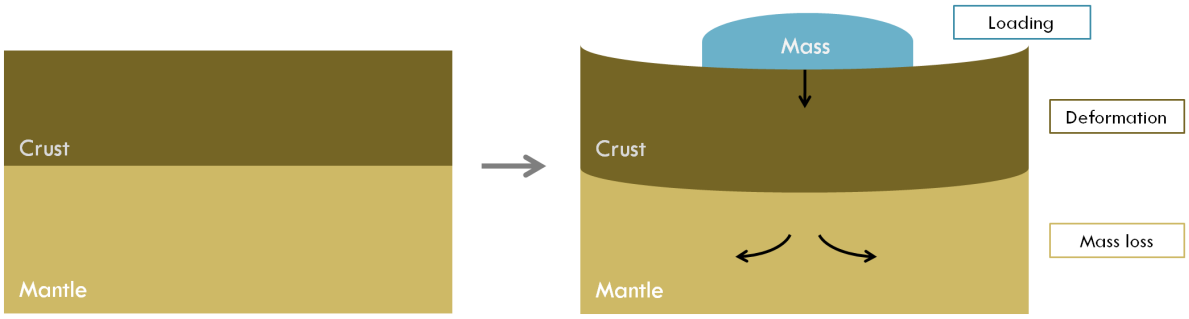

Figure 5: Schematic illustration of surface loading [Mayer-Gürr, 2012]

Due to surface loading (gain of mass), the Earth's crust deforms in the area of additional mass (see Fig. 5). This deformation indirectly changes the Earth's gravity field and is described with what is called the deformation potential V^{defo}. It can be expressed with the loading potential V^{load} by multiplying the loading potential with k'_n, a load Love number

$$V^{defo} = \sum_{n=0}^{\infty} k'_n V_n^{load} . \tag{10}$$

The dimensionless and degree-dependent load Love numbers (k', h' and l'), named after A. E. H. Love, represent the variation of the potential as well as the normalized vertical and horizontal displacement respectively. Thus, they describe the deformation of the Earth's figure due to loading. At this point it has to be mentioned that the Earth's figure is simplified by a radially symmetric elastic body [Rietbroek, 2014; Spada, 2008; Farrell, 1972].
Load induced deformation of the Earth's crust in direction of local level system's axis (*north*, *east*, *up*) can be calculated with the help of the loading potential V^{load}

$$\begin{aligned} \Delta r_{up}(\lambda,\vartheta) &= \frac{1}{g}\sum_{n=0}^{\infty} h'_n V_n^{load}(\lambda,\vartheta) \\ \Delta r_{north}(\lambda,\vartheta) &= -\frac{1}{g}\sum_{n=0}^{\infty} l'_n \frac{\partial V_n^{load}(\lambda,\vartheta)}{\partial\vartheta} \\ \Delta r_{east}(\lambda,\vartheta) &= \frac{1}{g}\sum_{n=0}^{\infty} l'_n \frac{\partial V_n^{load}(\lambda,\vartheta)}{\sin\vartheta\,\partial\lambda} . \end{aligned} \tag{11}$$

The load Love numbers h' and l' are used in equation (11), since they represent normalized vertical and horizontal displacement [Rietbroek, 2014].

2.4 Frame theory

When masses are redistributed on the Earth's surface, the center of mass of the solid Earth (CE) shifts in inertial space. It can also be observed that the center of mass of the Earth system (CM), which includes the solid Earth and the surface load, does not relocate due to surface loading. The difference between the CE and the CM is referred to as "geocenter motion" in this thesis.
Furthermore, only the degree-1 terms ($n = 1$) are dependent on the choice of the reference frame and therefore on the motion of the reference frame's origin relative to the deforming Earth (see chapter 2.2). Thus, the geocenter motion can be directly linked to degree-1 surface loading coefficients. When using "isomorphic reference frames", translations between reference frames can be realized by simply changing the degree-1 load Love numbers [Blewitt 2003; Farrell, 1972].

2.4.1 Isomorphic reference frames

In this subchapter, isomorphic frames as discussed in Blewitt (2003) are described. The reference frames are specified by load Love numbers as shown in table 2.

Center of Mass of the Earth System (CM) Frame. The entire Earth system includes the solid Earth and the surface loading. Consequently, the center of mass of the Earth system is not moving due to mass redistributions on Earth's surface in inertial system and the degree-1 term of the total potential of the temporal variation of the Earth's gravity field V_1^{total} (see chapter 2.3.1) yields zero. Therefore, the load Love number k_1' equals minus one

$$V_{CM,n=1}^{total} = \sum_{n=1}^{1}(1 + k_n')\, V_n^{load} = (1 - 1)\, V_n^{load} = 0\,. \tag{12}$$

As satellites orbit around the Earth's center of mass, the reference frame fixed to the CM is their natural choice of reference frames.

Center of Mass of the solid Earth (CE) Frame. This reference frame is fixed to the center of mass of the solid Earth. Therefore, when masses redistribute on the Earth's surface and the barycenter of the surface load changes, the CE moves in inertial space. It can also be seen that the trajectory of the CE does not change due to any resulting deformation of the solid Earth itself. Consequently, the load Love number k_1' and the deformation potential V_1^{defo} (see chapter 2.3.1) are set to zero in this frame

$$V_{CE,n=1}^{total} = \sum_{n=1}^{1}(1 + k_n')\, V_n^{load} = (1 - 0)\, V_1^{load} = V_1^{load}. \tag{13}$$

Because of these properties, this frame is suitable for modeling all dynamics of the solid Earth. Unfortunately, the CE frame is not directly approachable for observations. However, the center of surface figure (CF) frame, which is commonly used in geodetic pracitce, closely approximates (within 2 %) the CE.

Center of Surface Figure (CF) Frame. Imagine an infinite dense array of points in motion uniformly covering the Earth's surface. This array of points is geometrically defining the CF frame. The center of surface figure is defined so that the surface integral over all point displacements is zero (no-net translation). In practice, an infinite dense array of points is not realizable. Even if the GPS network has a globally dense distribution of geodetic sites, only a finite number of stations is available. Therefore, the term center of network (CN) has to be used instead of CF [Wu et al., 2012].

Center of Surface Lateral Figure (CL) Frame. This reference frame is defined by the condition that the surface integral over all points' horizontal displacements is zero. It can be used when vertical displacements have a lower accuracy then horizontal ones.
As can be seen in equation (11), the lateral displacements Δr_{north} and Δr_{east} include the l'_n load Love number. Consequently, the degree-1 values of this l'_n load Love number are set to zero in this frame (see table 2).

Center of Surface Height Figure (CH) Frame. A no-net height displacement condition defines the CH reference frame. This implies that the vector average of all points' vertical displacements on the Earth's surface is zero. To fulfill this condition, the degree-1 values of the h'_n load Love number are set to zero (see table 2).

Table 2: Specific degree-1 load Love numbers of isomorphic reference frames [Blewitt, 2003]

	CM	**CE**	**CF**	**CL**	**CH**
$\boldsymbol{k'_1}$	-1	0	0.021	-0.113	0.290
$\boldsymbol{h'_1}$	-1.290	-0.290	-0.268	-0.403	0
$\boldsymbol{l'_1}$	-0.887	0.113	0.134	0	0.403

Different perspectives. So far, the motion of the center of mass has only been discussed in inertial space, where the Center of Mass of the Earth System (CM) is not moving due to surface loading. However, this stationarity is not fulfilled when seen from another reference frame. In Fig. 6 the positions of the center of mass of the Earth system (CM) as well as of the center of mass of the solid Earth (CE) are displayed. The left column illustrates the motion of the CM and the CE due to loading in the Earth system frame and the satellite-based reference frame respectively. As discussed before, the CM as well as the satellite are stationary and the CE changes its position depending on the loading.
The right column displays the motion of the CM and the CE due to loading as seen from the solid Earth reference frame. Consequently, the CE is stationary and the CM as well as the satellite move depending on the loading.

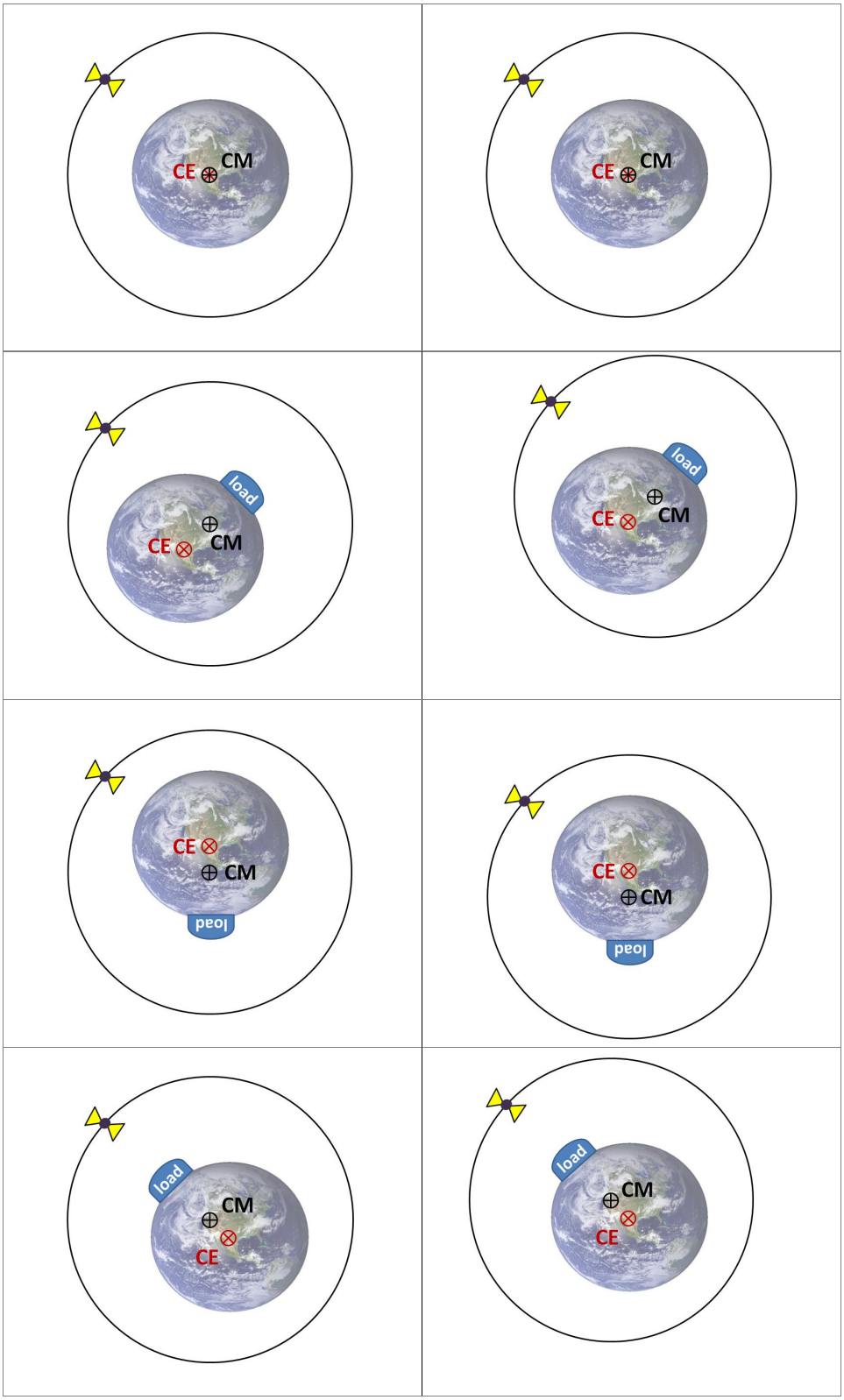

Figure 6: Schematic illustration of the motion of CE and CM

2.4.2 Isomorphic frame transformation

As mentioned before, isomorphic reference frames are defined by the choice of degree-1 load Love numbers. Thus, translating the origin of one frame into another can simply be realized by changing those load Love numbers. If they are given in one frame, they can be transformed into another frame by simply subtracting the dimensionless isomorphic parameter $\alpha^{A\to B}$

$$\begin{aligned} 1 + k_1'^B &= 1 + k_1'^A - \alpha^{A\to B} \\ h_1'^B &= h_1'^A - \alpha^{A\to B} \\ l_1'^B &= l_1'^A - \alpha^{A\to B}\,. \end{aligned} \tag{14}$$

Consequently, it can be seen that all origins of isomorphic reference frames lie on one straight line [Blewitt, 2003; Rietbroek, 2014]. This isomorphic parameter α is dependent on the reference frames between which the shift occurs. In equation (15) the isomorphic parameters for translations from an arbitrary isomorphic frame A into the earlier described isomorphic reference frames CM, CF, CE, CH and CL are displayed [Rietbroek, 2014]

$$\begin{aligned} \alpha^{A\to CM} &= 1 + k_1'^A \\ \alpha^{A\to CF} &= (h_1'^A + 2l_1'^A)/3 \\ \alpha^{A\to CE} &= k_1'^A \\ \alpha^{A\to CH} &= h_1'^A \\ \alpha^{A\to CL} &= l_1'^A\,. \end{aligned} \tag{15}$$

2.4.3 Geocenter motion

As defined in this thesis, the offset between the origin of the CM frame and the origin of the CE frame is described as "geocenter motion" and can be directly calculated from degree-1 surface loading coefficients (c_{10_load}, c_{10_load} and s_{11_load}). The difference between the origin of an isomorphic coordinate system (CX) and the center of mass of the Earth system (CM) can be calculated as follows:

$$\mathbf{X}_{CM} - \mathbf{X}_{CX} = (1 + k_1'^{CX}) \cdot \frac{3R}{\sqrt{3}} \cdot \begin{pmatrix} c_{11\_load} \\ s_{11\_load} \\ c_{10\_load} \end{pmatrix}. \tag{16}$$

The term $(1 + k_1'^{CX})$ in equation (16) equals the isomorphic parameter $\alpha^{A\to CM}$ described in equation (15) and causes the shift between the two reference frames. To determine the geocenter motion, the k_1 load Love number of the solid Earth (CE) frame ($k_1'^{CE} = 0$) was used in this formula [Rietbroek, 2014].

3 Methods

The geocenter motion is calculated with GPS and GRACE data in this thesis. Load induced degree-1 potential coefficients can be determined with the help of GPS station displacement observations. Because of the fact that GRACE satellites orbit the center of mass of the Earth system (CM), degree-1 coefficients cannot be directly calculated from GRACE observations. However, potential coefficients of degrees higher than one derived from GRACE observations are added to a combined least squares adjustment with GPS observations. This entails that low degree coefficients (including degree-1 terms) can be better separated and the geocenter motion can be determined more accurately [Rietbroek, 2014].

3.1 GPS Input Data

Firstly, the GPS input data is described in more detail. Not only the given GPS time series, but also the GPS data processing of this thesis are discussed.

3.1.1 Data information

Daily displacement data of IGS stations (see chapter 2.1.2) is used for calculations in this thesis. Those time series were downloaded from the Jet Propulsion Laboratory (JPL) website [JPL, 2014]. It has to be mentioned that for each station three files with each lateral (north), longitudinal (east) or radial (up) data are provided. Those local level data is given in centimeters. As earmarked on JPL's website, following background models were reduced from the observations during JPL's data processing:

> "Gravity from Earth, Sun, Moon, and other planets
> DE421 planetary ephemeris
> GSPM10 satellite solar pressure model
> IAU06 model for precession and nutation
> IERS2010 tides
> FES2004 ocean loading
> IGS satellite and receiver antenna phase center models" [JPL, 2014].

Detailed information on the estimated orbit and point positioning parameters can be found in the documentation about the applied methods on JPL's website [JPL, 2014].

3.1.2 Data processing

The downloaded GPS time series consist, among other things, of deformation movements caused by the Earth's mantle and crust. As the load induced geocenter motion is calculated in this thesis, those influences such as sudden movements (jumps) as well as drifts in the time series mainly caused by plate tectonics, would falsify the result and were therefore removed. It has to be pointed out that only data from January 2003 onwards was used, as GRACE data is only available from that year on. Moreover, IGS stations with data available for less then four years were not taken into account.
The GPS data processing was carried out for the lateral, longitudinal and radial displacement data of each station and was calculated with MATLAB.

Trend elimination. The trend can be determined, as discussed in Niemeier (2008), with the help of a polynomial fitting. The linear trend **m** was calculated with a polynomial of degree one

$$m(t) = \hat{x}_1 + \hat{x}_2 \cdot (t - t_0)\,. \tag{17}$$

The point in time t in equation (17) is representing one of the time epochs of the time series. The first epoch of the time series t_0 is subtracted of all other time epochs. The parameters $\hat{x}_1$ and $\hat{x}_2$ in equation (17) display the two elements of the parameter vector $\hat{\mathbf{x}}$ calculated by a least squares adjustment

$$\hat{\mathbf{x}} = (\mathbf{A^T P A})^{-1} \cdot \mathbf{A^T P l} = \mathbf{N^{-1}} \cdot \mathbf{n}\ . \tag{18}$$

As the trend vector is calculated for each time series separately, the observation vector **l** in equation (18) consists either of the north, east or up movement data of one IGS station. The design matrix **A** is given as follows:

$$\mathbf{A} = \begin{bmatrix} 1 & t_1 - t_0 \\ \cdot & \cdot \\ \cdot & \cdot \\ 1 & t_i - t_0 \end{bmatrix}\ . \tag{19}$$

Due to the differentiation in the second column of the design matrix **A**, the values of this matrix have approximately the same magnitude and therefore the least squares adjustment is more stable. At this point it has to be mentioned that no weights were used in the least squares adjustment. Consequently, the weight matrix **P** is replaced by an identity matrix **I**. Moreover, the normal matrix **N** displays the product $\mathbf{A^T PA}$.
The calculated linear trend vector **m** can then be subtracted from the observation vector **l**. This difference is denoted as detrended observation vector l_{elim}

$$\mathbf{l}_{elim} = \mathbf{l} - \mathbf{m}\ . \tag{20}$$

Jump detection. As some of the given GPS time series consist of jumps, a trend determination of the entire time series would falsify the result. Thus, when the exact positions of the jumps are known, a linear trend can be calculated for each interval.
However, to determine the differences between the values of the time epochs more easily, the drift of the given time series can be removed before jump detection. It only has to be ensured that the original data is used for the final trend elimination.
Furthermore, as the radial component of the given time series is noisier than the lateral and longitudinal one, a centralized moving average filter, with an interval length of 12 days, was applied to the radial time series.

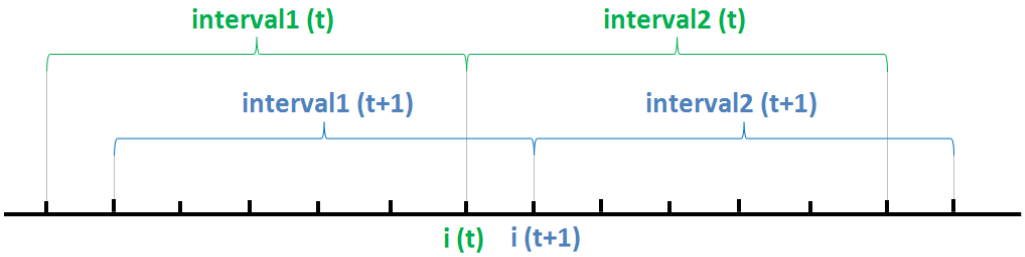

Figure 7: Schematic illustration of interval formation

As GPS data has a certain noise, it is not possible to simply differentiate the values between successive time epochs to get information of the eventual presence of jumps. This is why for each point in time i two intervals of the same length were defined; The first one ending at the point in time i and the second one starting at i (see Fig. 7). The interval length was set to 50 days for the lateral and longitudinal time series and to 3 days for the radial time series. In the next step, the mean value of each interval was calculated. The subtraction of those mean values provides information about the presence of a jump. In this thesis, a difference bigger than the value of 0.7 centimeters was defined as a jump. This procedure has to be carried out for every point in the entire time series.

Due to the interval formation, one jump is detected at several successive points in time. This epoch could be denoted as a "group of jump". If there are more jumps existing in the time series, several of those groups exist. Therefore, the groups have to be separated from each other first and then the actual position of the jump has to be detected.
As the groups have different time epochs, it is simple to separate them from each other. The correct position of the jump in one group can be detected with the help of the detrended time series. Firstly, the time intervals of the "groups of jump" have to be found in the detrended time series. Secondly, the differences of the values in those intervals have to be calculated and the maximum of those differences is the actual position of the jump.

Trend and outlier removal. After having detected the jumps, a correct trend elimination can be realized as described at the beginning of this subchapter. If two jumps occur in an interval of less then 70 days, the data in between the jumps was set to NaN. Consequently, no trend could be determined for this time epoch. Furthermore, outliers were removed with the help of the 3σ test

$$x_{outlier} = x > 3 \cdot \sigma_{timeseries} \ . \tag{21}$$

After having removed trend and outliers, the data was saved in files. As it is more convenient for further calculations, a file for each day consisting of north, east and up displacement data of all available stations was created.

3.2 GRACE Input Data

Daily potential coefficients c_{nm} and s_{nm} derived from GRACE observation data were used for calculations. The coefficients were provided by the Institute of Theoretical Geodesy and Satellite Geodesy of Graz University of Technology [Mayer-Gürr et al., 2014].
The following background models were reduced during GRACE data processing:

"Background models:

- Earth rotation IERS2003 (EOP_08C04_IAU2000)
- Static field: GOCO03s
- Trend, Annual, Semiannual: from ITG-Grace2010 (degree n=40, filtered)
- Third body forces (sun, moon, planets): JPL DE421
- Solid earth tides: IERS 2003
- Ocean tides: EOT11a (max. degree n=120)
- Pole tides: IERS 2003
- Ocean pole tides: Desai 2004 (max. degree n=120)
- Atmospheric tides (S1, S2) Bode-Biancale 2003
- Dealiasing: AOD1B RL05 (Atmospheric S2 removed)
- non conservative forces: Accelerometer (scaled)" [Mayer-Gürr et al., 2014].

Detailed information on the estimated parameters can be found in the documentation about the applied methods [Mayer-Gürr et al., 2014].

3.3 Combined Least Squares Adjustment

In this chapter the combined least squares adjustment is described. Daily degree-1 loading potential coefficients c_{10_load}, c_{11_load} and s_{11_load} shall be determined with the help of GPS deformation movements and GRACE loading potential coefficients of degrees higher than one. Those calculations were realized in C++ and implemented into "GROOPS", the software of the Institute of Theoretical Geodesy and Satellite Geodesy (Graz University of Technology).

Preprocessing. To be able to process a combined least squares adjustment, some preprocessing steps had to be implemented. Firstly, as the ocean and atmospheric dealiasing product as well as the annual and semi-annual trend were already removed from GRACE data, they had to be eliminated from the GPS data as well. It has to be mentioned that those two background models were removed starting with degree two and therefore this processing step does not effect the degree-1 loading potential coefficients.
Secondly, as daily GRACE solutions are used and a global coverage is only available on a monthly basis, a regularization had to be applied to the GRACE data. This was realized by adding a regularization normal equation to the least squares adjustment.
Thirdly, to be able to calculate the degree-1 loading potential coefficients correctly, all input data of the least squares adjustment has to be given for the loading potential V_{load}. As the GRACE normal matrix $\mathbf{N_G}$ as well as the regularization normal matrix $\mathbf{N_{reg}}$ are given for the total potential V_{total}, they had to be converted. The difference between the loading and the

total potential is the deformation potential (see chapter 2.3.2) and therefore this conversion can be realized as follows:

$$\mathbf{N}_{load}^{-1} = \text{diag}\left(\frac{1}{1+k_n}\right) \cdot \mathbf{N}_{total}^{-1} \cdot \text{diag}\left(\frac{1}{1+k_n}\right) \ . \tag{22}$$

Least squares adjustment. After preprocessing, all data can be used in one least squares adjustment

$$\hat{\mathbf{x}} = (\mathbf{A^T P A})^{-1} \cdot \mathbf{A^T P l} = \mathbf{N^{-1}} \cdot \mathbf{n} \ . \tag{23}$$

The unknown parameter vector $\hat{\mathbf{x}}$ consists of loading potential coefficients c_{nm_load} and s_{nm_load} from degree one up to degree 40 and of seven Helmert parameters. The Helmert transformation parameters t_x, t_y, t_z (translation), s (scale) and r_x, r_y, r_z (rotation) are estimated together with the loading potential coefficients and represent deformation movements not caused by surface loading. The observation vector $\mathbf{l}$ consists of GPS station movements Δr_{north}, Δr_{east} and Δr_{up} of all IGS stations taken into account (St_1 to St_n) as well as of GRACE loading potential coefficients of degrees higher than one.

The relation between the given deformation movements Δr_{north}, Δr_{east} and Δr_{up} and the unknown loading potential coefficients c_{nm_load} and s_{nm_load} is given in equation (11). Therefore and because of the given GRACE data and the to determining Helmert parameters, the design matrix $\mathbf{A}$ can be displayed as follows:

$$\mathbf{A} = \begin{pmatrix} \mathbf{A_{GPS}}(deg1)[St1] & \mathbf{A_{GPS}}(>deg1)[St1] & \mathbf{A^{local}_{Helmert}}[St1] \\ \mathbf{A_{GPS}}(deg1)[St2] & \mathbf{A_{GPS}}(>deg1)[St2] & \mathbf{A^{local}_{Helmert}}[St2] \\ \vdots & \vdots & \vdots \\ \mathbf{0} & \mathbf{I} & \mathbf{0} \end{pmatrix} . \tag{24}$$

As can be seen in equation (24), the design matrix $\mathbf{A}$ can be divided in three groups of columns. The first two groups display the relation between the loading coefficients and the observations. The first block of rows of those two groups represents the relation between the given GPS deformation movements and the unknown loading potential coefficients. This

relation can be displayed for each station:

$$\mathbf{A_{GPS}}(St) = \begin{pmatrix} -\frac{GM}{gR} l_1 \frac{\partial P_{10}(\cos\vartheta_{St})}{\partial\vartheta} & -\frac{GM}{gR} l_1 \frac{\partial P_{10}(\cos\vartheta_{St})}{\partial\vartheta} \cos\lambda_{St} & \dots \\ 0 & -\frac{GM}{gR} \frac{l_1}{\sin\vartheta_{St}} P_{11}(\cos\vartheta_{St}) \sin(\lambda_{St}) & \dots \\ \frac{GM}{gR} h_1 C_{10}(\lambda_{St}, \vartheta_{St}) & \frac{GM}{gR} h_1 C_{11}(\lambda_{St}, \vartheta_{St}) & \dots \end{pmatrix}. \quad (25)$$

The second block represents the relation between the given GRACE loading coefficients and the unknown loading coefficients. As GRACE data cannot be directly used to calculate degree-1 terms, the first three columns of this block (degree-1) are set to zero. The other columns define the relation between all loading coefficients higher than degree-1 and the input data. As GRACE input data is used one to one to calculate the loading coefficients, those columns are represented by an identity matrix **I**.
The last columns of matrix **A** in equation (24) define the relations to calculate the seven Helmert parameters. Because of the fact that the GRACE data does not influence those parameters, the second block of rows is set to zero. The first block of rows of those last columns represent the relation between the Helmert parameter and the station deformation and can be calculated for each station as follows:

$$\mathbf{A_{Helmert}}(St) = \begin{pmatrix} 1 & 0 & 0 & x_{St} & 0 & z_{St} & -y_{St} \\ 0 & 1 & 0 & y_{St} & -z_{St} & 0 & x_{St} \\ 0 & 0 & 1 & z_{St} & y_{St} & -x_{St} & 0 \end{pmatrix}. \quad (26)$$

Moreover, as the GPS station movements are given in the local level system, the matrix $\mathbf{A_{Helmert}}$ has to be transformed into that system [Hofmann-Wellenhof et al., 2008]

$$\mathbf{A^{local}_{Helmert}}(St) = \begin{pmatrix} -\sin\varphi_{St}\cdot\cos\lambda_{St} & -\sin\lambda_{St} & \cos\varphi_{St}\cdot\cos\lambda_{St} \\ -\sin\varphi_{St}\cdot\sin\lambda_{St} & \cos\lambda_{St} & \cos\varphi_{St}\cdot\sin\lambda_{St} \\ \cos\varphi_{St} & 0 & \sin\varphi_{St} \end{pmatrix}^T \cdot \mathbf{A_{Helmert}}(St). \quad (27)$$

In addition to the given weights, a variance component estimation was realized to determine the respective contribution of GPS and GRACE input data to the solution. For detailed calculation steps see Niemeier (2008).

3.4 Parametrization

After having estimated the loading potential coefficients of degree-1 with a combined least squares adjustment, it is possible to compute the geocenter motion (see section 2.3.2)

$$\mathbf{X}_{CM} - \mathbf{X}_{CE} = (1 + k_1^{'CE}) \cdot \frac{3R}{\sqrt{3}} \cdot \begin{pmatrix} c_{11\_load} \\ s_{11\_load} \\ c_{10\_load} \end{pmatrix}. \tag{28}$$

As the geocenter motion is defined as the offset between the Center of Mass of the Earth System (CM) and the Center of Mass of the solid Earth (CE), the k_1' load Love number of the CE Frame ($k_1^{'CE} = 0$) was used in equation (28).
Furthermore, the seven Helmert parameters are already part of the parameter vector in the least squares adjustment and therefore only have to be scaled to the purposely unit.

4 Results

In this chapter the results of this thesis are discussed. At the beginning, the detected jumps as well as estimated trends of the given GPS time series are displayed. Secondly, the computed geocenter motion and Helmert parameters are illustrated. Moreover, the influences of the GPS station distribution, the used degree-1 load Love number as well as the contribution of GRACE data are discussed. The last subchapters display the GPS-only solution as well as the influences of the GPS accuracy specifications.

4.1 GPS data processing

As discussed in chapter 3.1, a data processing of the given GPS time series was implemented. It includes a jump detection, a trend elimination as well as an outlier removal.
Data of 177 globally distributed IGS stations was taken into account for calculations. However, not all of those time series contain jumps. Because of this, only the results of two representative IGS stations (with jump) are displayed in this chapter. In Fig. 8 all IGS stations, of which data was used, as well as the two IGS stations discussed in this chapter are displayed. Those two stations, which are marked with a star, are on the one hand "KERG" on Kerguelen Islands in the southern Indian Ocean and on the other hand "MTBG" in Mattersburg, Austria.
Their time series as well as the trend and the detected jumps are displayed in Fig. 9 and Fig. 10. The original time series is displayed in red, the calculated trend in black and the positions of jumps in blue. It should be noted that the jumps in the time series of those two stations do not have geophysical reasons. The jump in time series of the station located on Kerguelen Islands (KERG) is caused by a change of the receiver antenna [IGS, 2014].

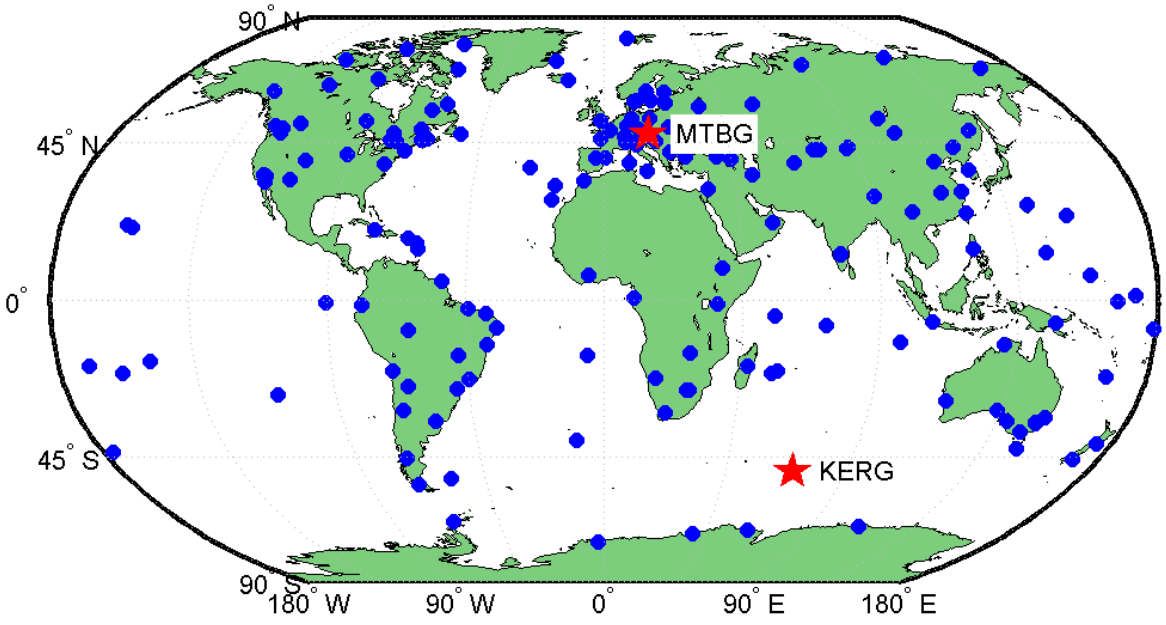

Figure 8: Map of IGS station positions

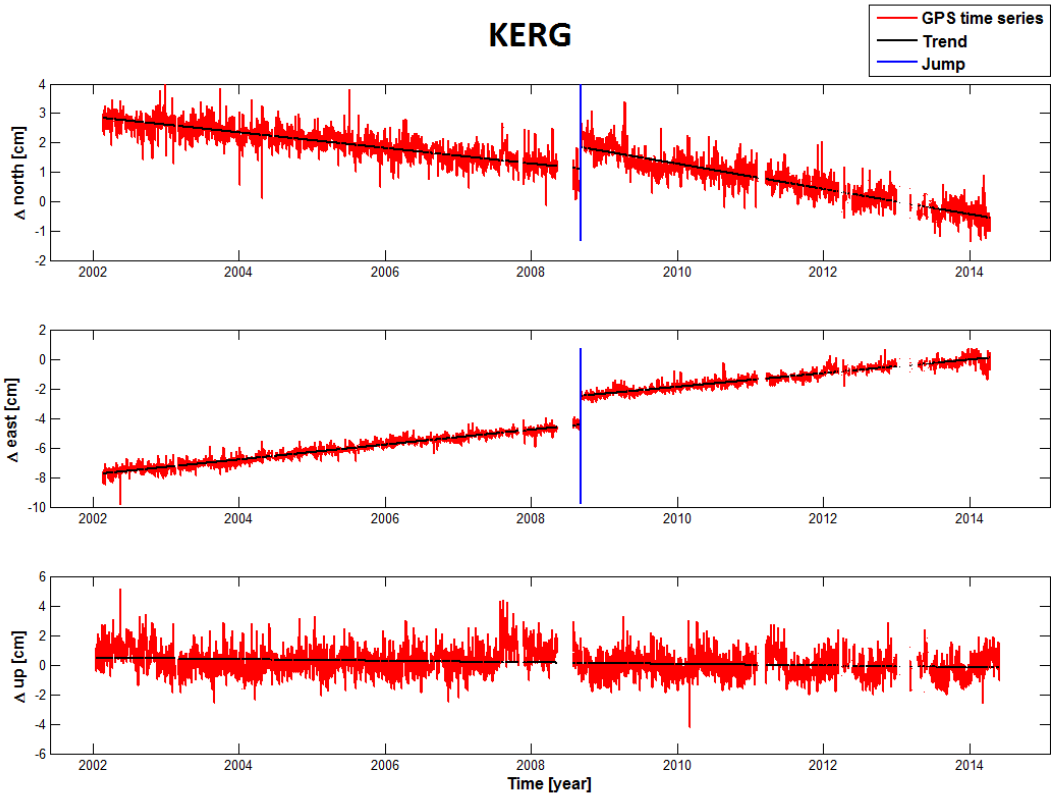

Figure 9: GPS time series of the IGS station "KERG"

The data of Mattersburg's station shows three jumps. Two of them in the up component and one in the east component (see Fig. 10). It seems as if some receiver problems occured at this station. The receiver's firmware was changed on October 10th, 2008. This is the point in time when the second jump in the up component appears. Consequently, it is not far to seek that the first jump in the up component was the reason for changing the firmware. For more details see IGS (2014). Unfortunately, the reason for the jump in the east component is mentioned neither in any log file nor in any recording of geophysical phenomena. The jump occurred in January 2009, when a perishing cold dominated Austria. As the GPS antenna of this station is mounted on the roof of an older building, frost could have caused a lateral movement [IGS, 2014; ZAMG, 2014]. It is also likely that the cold temperatures caused problems in the antenna.
Furthermore, it can be seen in Fig. 9 and Fig. 10 that the trend of a time series was estimated separately before and after a jump. This is essential, as the data has to be detrended correctly for further calculations. It should also be mentioned that the detection of jumps was computed for each component (north, east and up) separately. This was important, as most of the jumps do not appear in all three components (see e.g. Fig. 10).

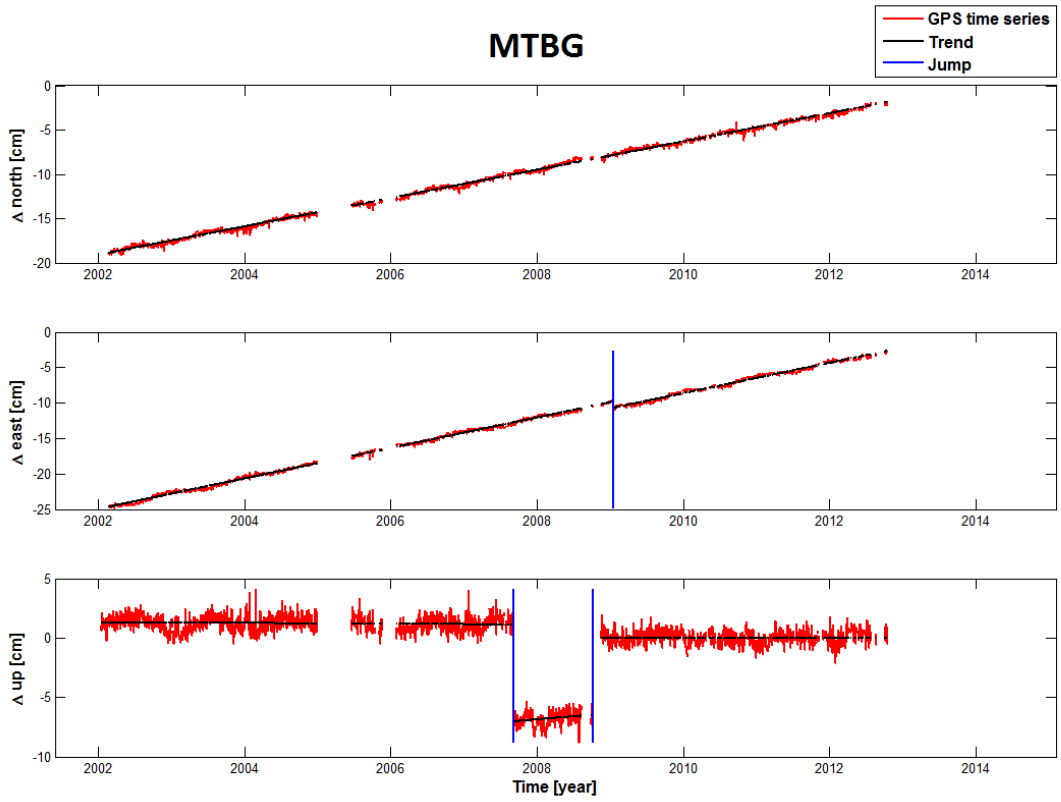

Figure 10: GPS time series of the IGS station "MTBG"

After having removed the trend from all given GPS time series correctly, a 3σ outlier removal has to be realized. In Fig. 11 and Fig. 12 the detrended time series of the IGS stations "KERG" and "MTBG" are displayed in blue and their outliers in red. After eliminated these outliers, the GPS data processing is completed and the data can be used for the combined least squares adjustment (see chapter 3).
When having a closer look at the detrended time series in Fig. 11 and Fig. 12, some interesting characteristics can be observed. The time series of the station on Kerguelen Islands shows no seasonal changes, the data from the Austrian station, however, does. This can be explained by the climate zones in which the two stations are located. Port-aux-Français on Kerguelen Islands, a research station where "KERG" is based, has a tundra climate moderated by the ocean. The temperature is relatively stable throughout the year and snowfalls as well as heavy rain are very likely in summer as well as in winter [Prudent-Richard, 2009]. Because of this, no specific seasonal mass redistribution happens and the time series remain relatively stable. In contrast to that, the station "MTBG" is located in Central Europe, where seasons are an essential part of the climate. Because of this, annual cycles can be detected in the station's time series, as it moves due to seasonal loading (e.g. gain of mass due to snow).

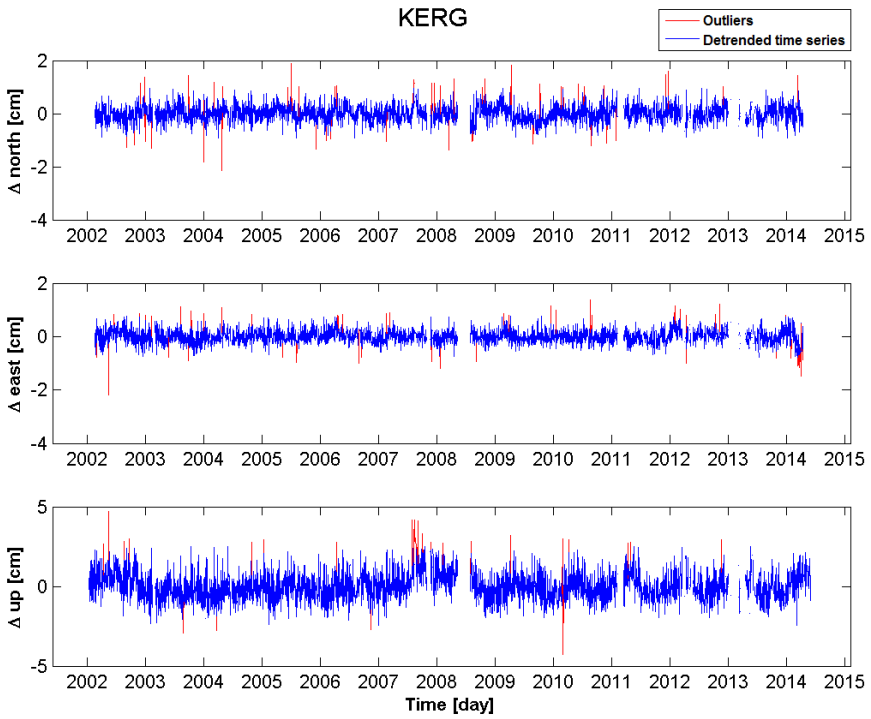

Figure 11: Detrended GPS time series of the IGS station "KERG"

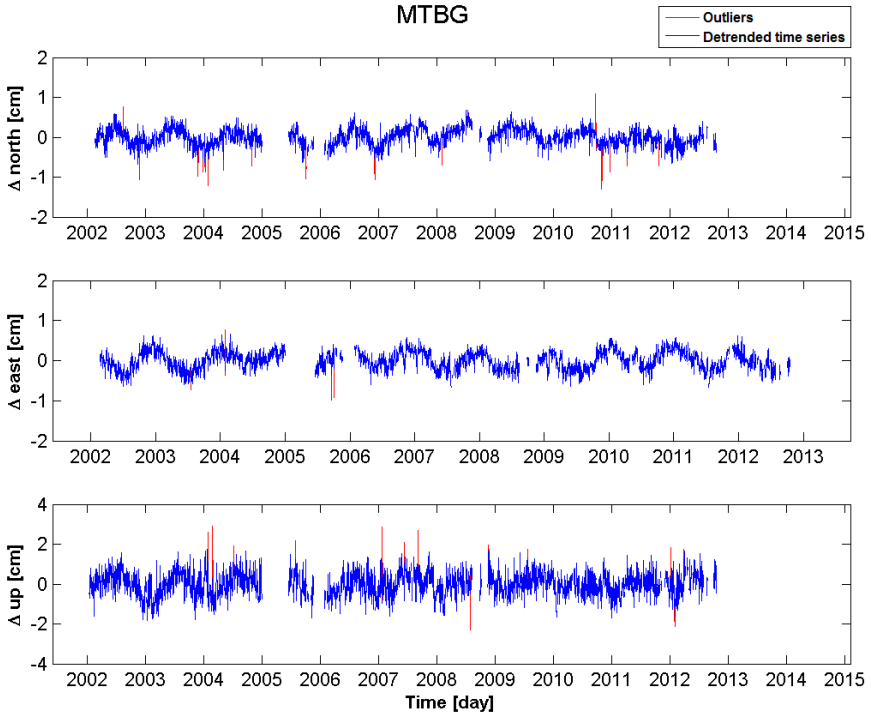

Figure 12: Detrended GPS time series of the IGS station "MTBG"

4.2 Geocenter motion and Helmert parameters

After the GPS data processing was completed, the combined least squares adjustment could be performed. The CE degree-1 load Love numbers were used in equation (25). With the help of the estimated degree-1 loading potential coefficients, the geocenter motion could then be computed.
In Fig. 13 the geocenter motion (CM-CE) is displayed in blue. For comparison purposes, the geocenter motion calculated by Rietbroek et al. (2012) is also illustrated in this figure. It can be seen, that the two time series are not exactly the same. Firstly, this may be the result of the fact that the geocenter motion was calculated for each day in this thesis, whereas the result of Rietbroek et al. (2012) is only a weekly solution. Secondly, the choice of GPS input data is very important for calculations and therefore different GPS input data can lead to different solutions. Additionally, in contrast to this thesis, modeled ocean bottom pressure (OBP) was used as a third input data set by Rietbroek et al. (2012).
To be able to compare the time series in detail, the annual aplitude and phase are displayed in table 3. The solutions of Swenson et al. (2008) and Cheng et al. (2010) are listed as well. It has to be mentioned that all results in table 3 are based on the geocenter motion time series reduced by the dealising product. It can be seen that the results of this thesis (denoted as "Geocenter motion") are in the dimension of the other solutions.

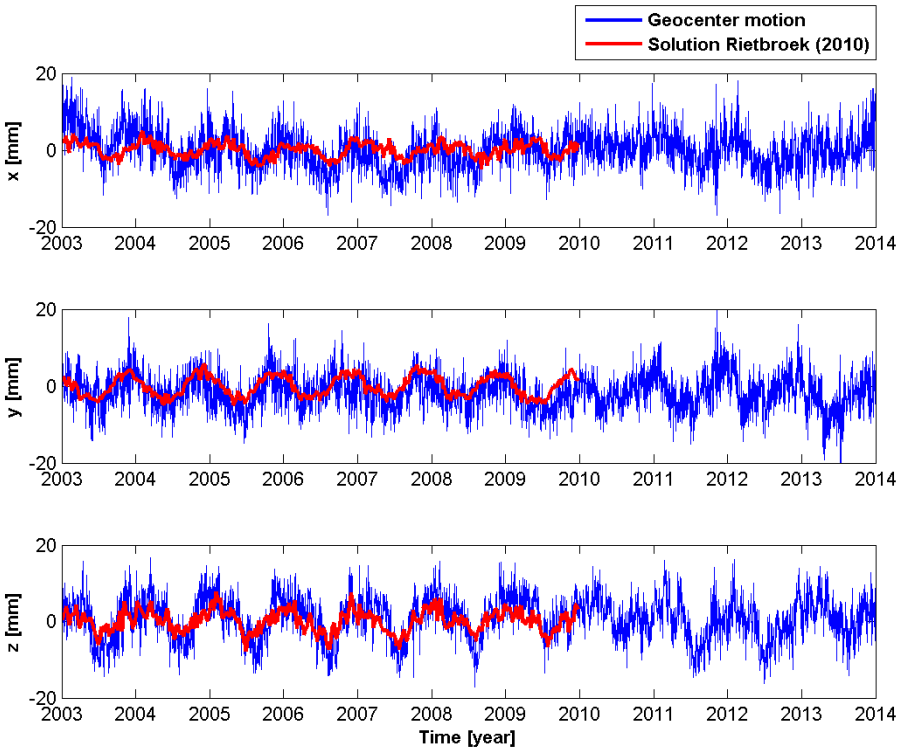

Figure 13: Geocenter motion

Table 3: Annual amplitude and phase [based on Rietbroek (2014)]

Solution		**Annual Amplitude [mm]**	**Annual Phase [doy]**
Geocenter motion	x:	1.5 (± 0.10)	34 (± 4)
	y:	1.8 (± 0.09)	312 (± 3)
	z:	4.3 (± 0.09)	45 (± 1)
Rietbroek (2014)	x:	1.3 (± 0.06)	137 (± 3)
	y:	2.2 (± 0.06)	304 (± 2)
	z:	2.5 (± 0.06)	72 (± 1)
Rietbroek et al. (2012)	x:	1.5 (± 0.07)	107 (± 3)
	y:	2.2 (± 0.05)	305 (± 1)
	z:	2.3 (± 0.09)	32 (± 2)
Swenson et al. (2008)	x:	1.7 (± 0.07)	99 (± 3)
	y:	1.2 (± 0.07)	283 (± 4)
	z:	2.3 (± 0.10)	93 (± 3)
Cheng et al. (2010)	x:	2.8 (± 0.35)	40 (± 7)
	y:	0.6 (± 0.39)	318 (± 36)
	z:	4.4 (± 0.48)	50 (± 6)

Furthermore, Helmert transformation parameters t_x, t_y, t_z (translation), s (scale) and r_x, r_y, r_z (rotation) were estimated. The values are displayed in Fig. 14. It can be seen that especially the values in the years 2010 to 2013 have fluctuating magnitudes. This may be explained by the number of IGS stations, of which data was used for calculations. As not all sites are providing data every day, it can happen that the number of available stations alternates. In Fig. 15 this number of stations available is displayed for each time epoch. It can be seen that in average, data of approximately 140 stations is used for calculations. However, especially in the years 2010 to 2013 the number of sites is not constant over time. As the geometrical distribution influences the Helmert transformation parameters, some fluctuations in the magnitude can be observed in those time series.

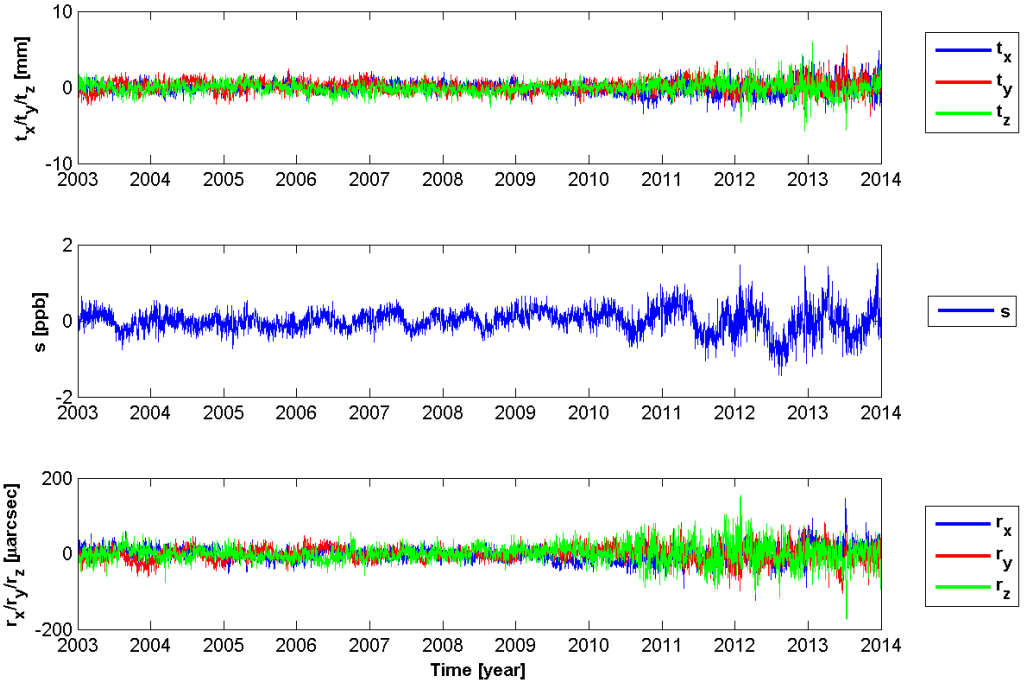

Figure 14: Helmert transformation parameters

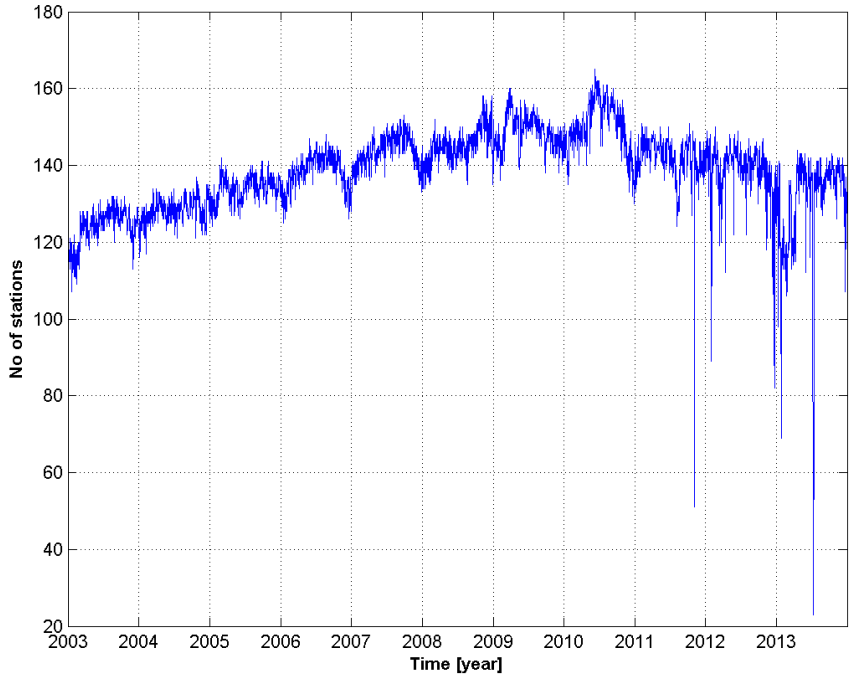

Figure 15: Number of stations used

4.2.1 Influences of degree-1 load Love numbers

As discussed before, the degree-1 loading potential coefficients were calculated with GPS deformation observations. This could be done with the help of equation (11). As can be seen, load Love numbers are part of this equation. The CE frame is suitable for modeling all dynamics of the solid Earth and therefore CE load Love numbers were used to estimate loading potential coefficients and consequently the geocenter motion.
However, the influences on the solution when using load Love numbers of the CM reference system have yet to be determined. In Fig. 16 the difference between the geocenter motion calculated with CE load love numbers and the geocenter motion calculated with CM load love numbers is displayed. Those differences may be neglected, since they are under the accuracy range. Consequently, it can be said that the solution of the geocenter motion is the same and that it does not make any difference whether the loading potential coefficients are calculated in the CE or the CM frame.
Helmert transformation parameters calculated with CM load Love numbers are displayed in Fig. 17. When comparing these results to the Helmert transformation parameters calculated with CE load Love numbers, clear differences in the translation parameters can be observed (see Fig. 18). As the GPS input data is apparently given in the CE frame, the translation parameters are close to zero when using CE load Love numbers (see Fig. 14). When using CM load love numbers, an additional translation occurs, which explains the difference. As only a translation differs the CE and the CM, the differences of scale and rotation are (close to) zero.

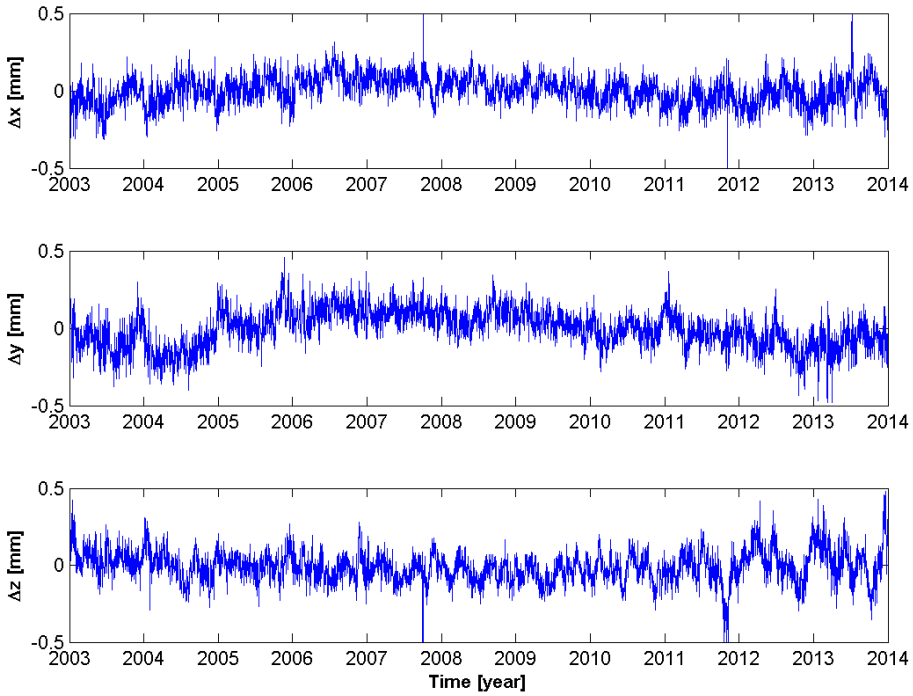

Figure 16: Difference of geocenter motions (CM-CE)

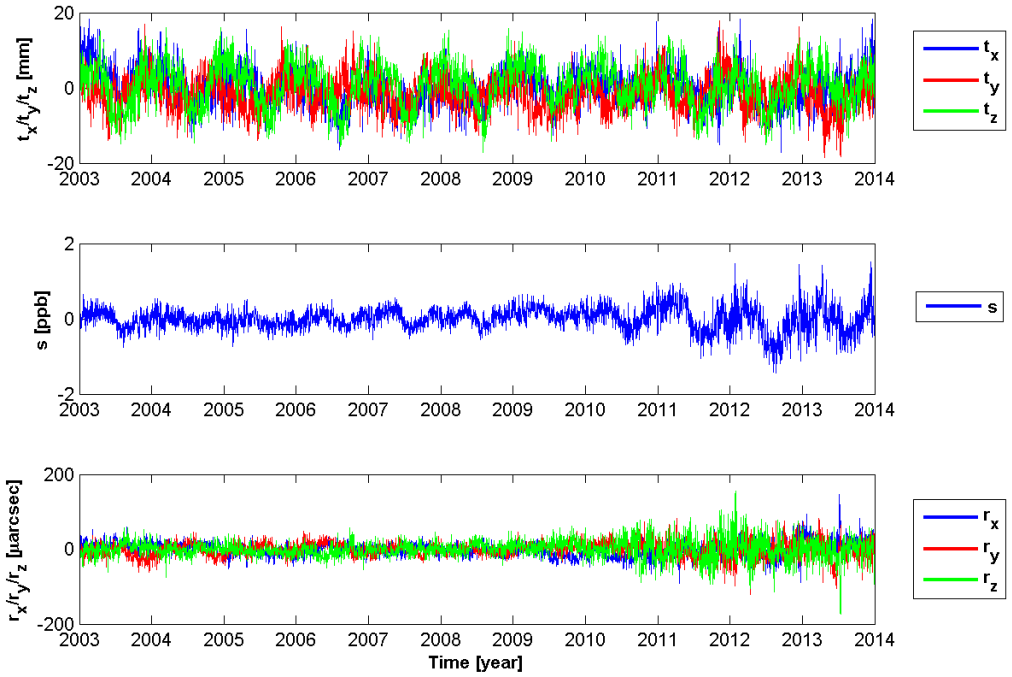

Figure 17: Helmert transformation parameters (CM)

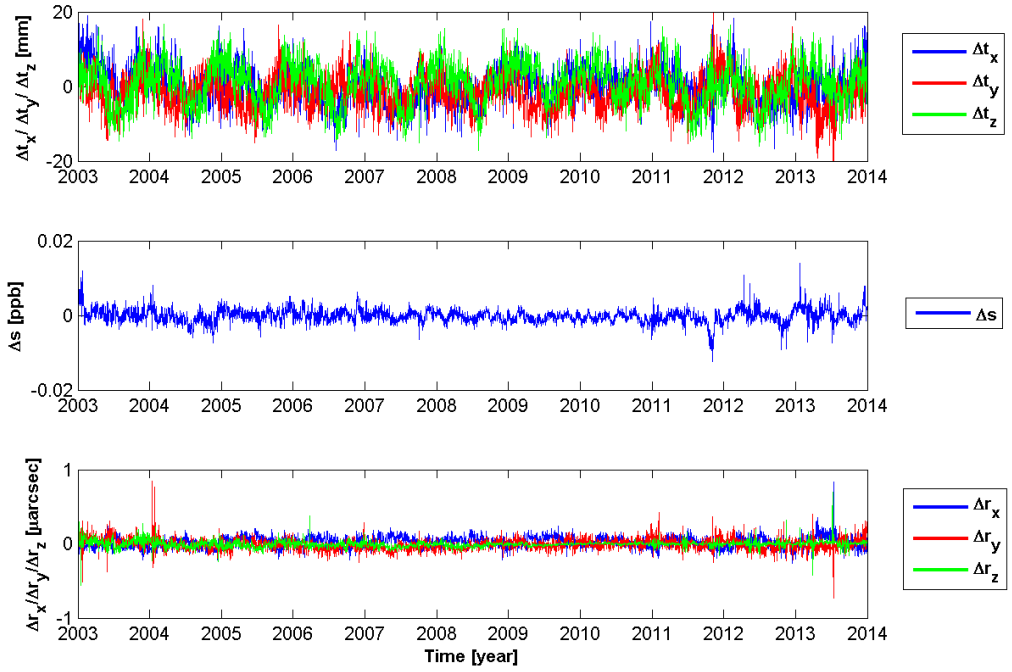

Figure 18: Difference of Helmert transformation parameters (CM-CE)

4.2.2 Influences of GPS station distribution

Usually, as many observations as possible are used to estimate parameters. However, when calculating the geocenter motion this does not have to be the case. The geocenter motion is defined as the offset between the origin of the Center of Mass of the Earth System (CM) frame and the origin of the Center of Mass of the solid Earth (CE) frame. The loading potential coefficients are calculated in the CE frame (as CE degree-1 load Love numbers are used) and with the help of equation (28) the distance to the CM was calculated. As the CE cannot be directly observed, it is approximated by the Center of surface figure (CF). The CF frame is geometrically defined by an infinite dense array of points covering the Earth's surface. Although the IGS GPS station network is globally well distributed, an infinite dense array of sites is not realizable. Therefore, the term Center of Network (CN) has to be used. When having a finite number of stations on the Earth's surface, it is important that they are well distributed so that the CN approximates the CF and therefore also the CE. This was implemented as can be seen in Fig. 8. However, it has to be kept in mind that there are only GPS sites on the continents and consequently an even global distribution can never be achieved.
The influence of the GPS station distribution on the result has yet to be analyzed. In contrast to Fig. 8, all GPS stations with data usable for this thesis are displayed in Fig. 19. It can be seen that in Europe and North America many more stations are located than anywhere else in the world. Therefore, it can be clearly said that the IGS sites are not very well distributed. With the data of all of those stations, the geocenter motion was calculated and is displayed in Fig. 20.

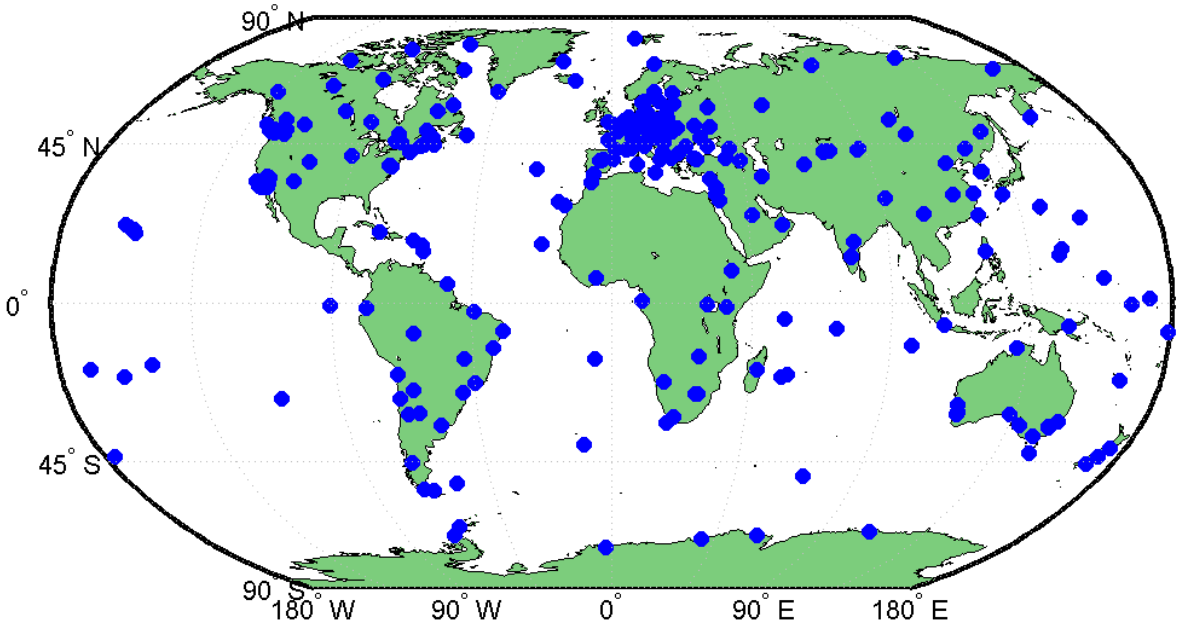

Figure 19: Map of IGS station positions

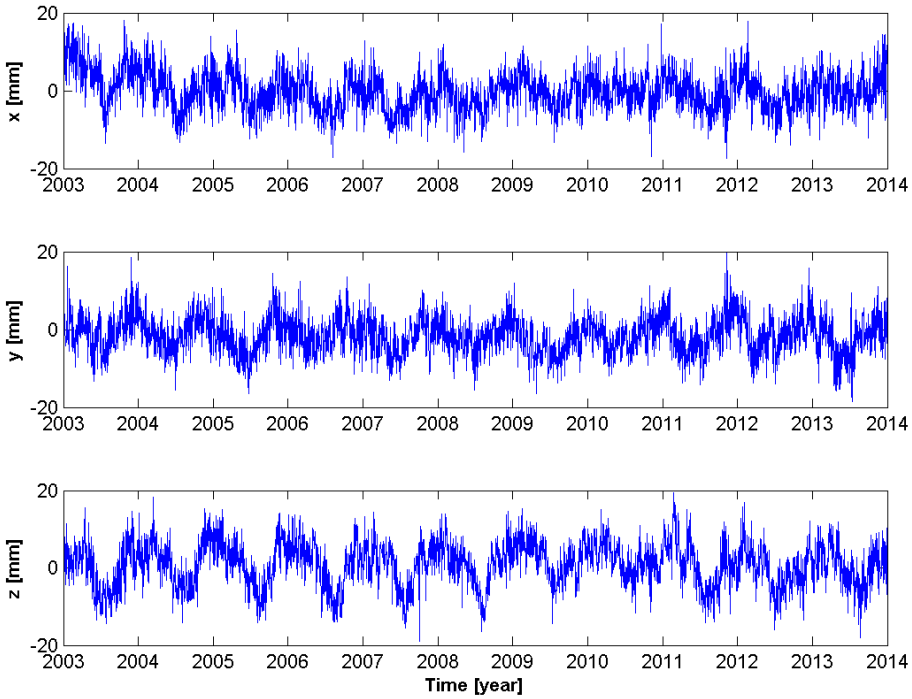

Figure 20: Geocenter motion calculated with data from all available stations

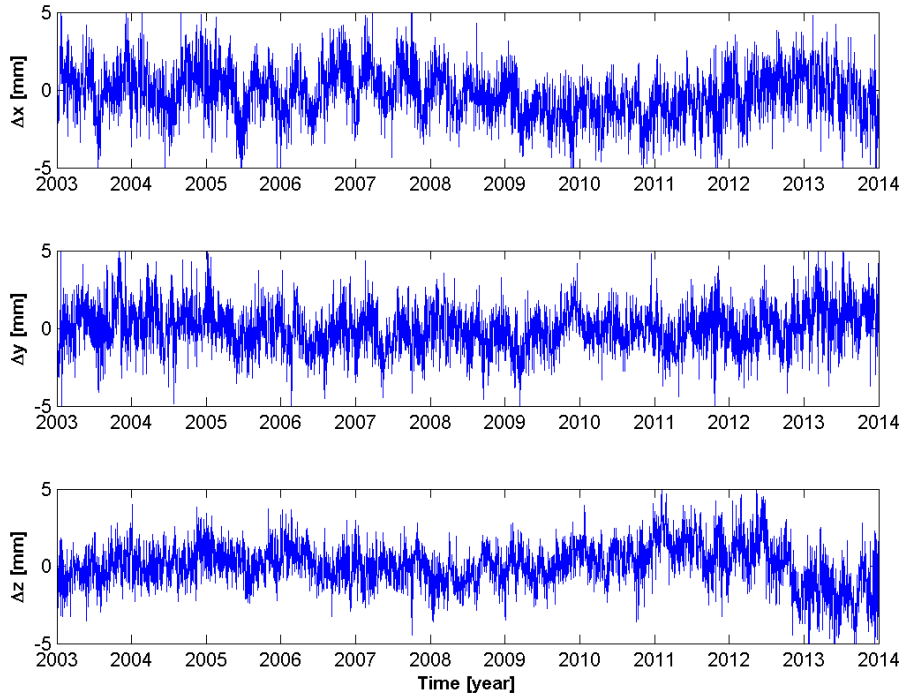

Figure 21: Difference of geocenter motions (all stations - final solution)

Table 4: Annual amplitude and phase of calculated geocenter motion

Solution		**Annual Amplitude [mm]**	**Annual Phase [doy]**
Geocenter motion	x:	1.5 (± 0.10)	34 (± 4)
	y:	1.8 (± 0.09)	312 (± 3)
	z:	4.3 (± 0.09)	45 (± 1)
Geocenter motion	x:	1.7 (± 0.10)	27 (± 4)
(all stations)	y:	2.0 (± 0.09)	315 (± 3)
	z:	4.5 (± 0.09)	45 (± 1)

Furthermore, the difference between this solution and the final solution with globally well distributed stations (displayed in Fig. 13) is illustrated in Fig. 21. As can be seen, the differences are in the magnitude of a few millimeters. When having a closer look at the amplitude and phase of the time series in table 4, it can be observed that they hardly show any differences. Consequently, it can be said that the distribution of GPS stations influences the result only up to a certain extent. Especially when considering that the sites are extremely unevenly distributed on the Earth's surface (see Fig. 19), the differences can be seen as quite small. Therefore, is is legitimate to calculate the geocenter motion with GPS stations distributed as displayed in Fig. 8, even if less stations are located in oceanic areas.

Furthermore, the differences of the estimated Helmert parameters are displayed in Fig. 22. Compared to Fig. 18 not only the translation but also the scale and rotation show differences. This can be explained by the fact that other or rather more stations were used which have a different distribution on the Earth's surface.

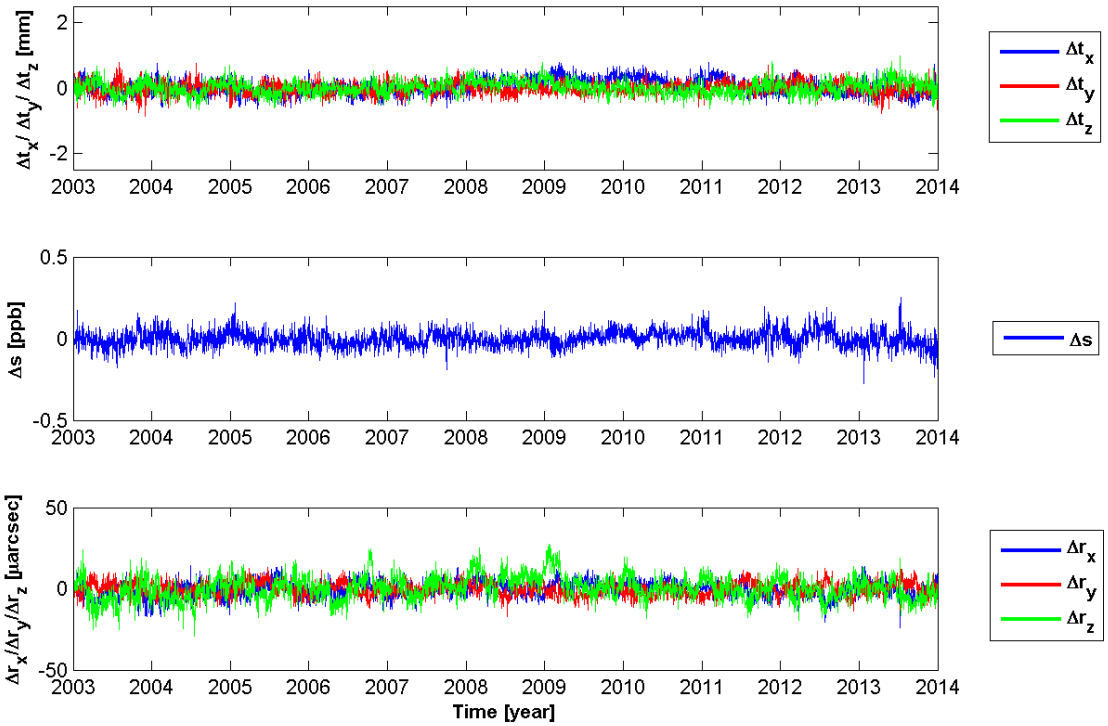

Figure 22: Differences of Helmert transformation parameters (all stations - final solution)

4.2.3 Contribution of GRACE and regularization data

As a combined least squares adjustment was realized in this thesis, it is interesting to determine the contribution of the different inputs with regard to the result. As discussed in chapter 3, GPS and GRACE data were used to determine loading potential coefficients up to degree 40. Additionally, a regularization had to be applied to the GRACE data as the calculations are based on daily data. In Fig. 23 the contributions of GPS, GRACE and regularization data to the estimated loading potential coefficients c_{nm} and s_{nm} are displayed for February 1st, 2003. The y-axis of each plot represents the degree n and the x-axis the order m. Coefficients displayed with a negative order m are denoted in this thesis as s_{nm} and those with a positive order (including zero) c_{nm}. Moreover, each graphic in Fig. 23 contains a detailed plot of the contributions to the first three degrees. As expected, only GPS data contributes to the solution of degree-1 loading potential coefficients. With GPS data only a low resolution is possible. Consequently, all other degrees are dominated by GRACE input data as well as by the regularization respectively. The latter mainly contributes to higher degrees, as daily GRACE data only has a good resolution up to a certain degree.
Furthermore, it should be mentioned that only the GPS input data contributes to the solution of the computed Helmert transformation parameters, as they represent deformation movements not caused by surface loading.

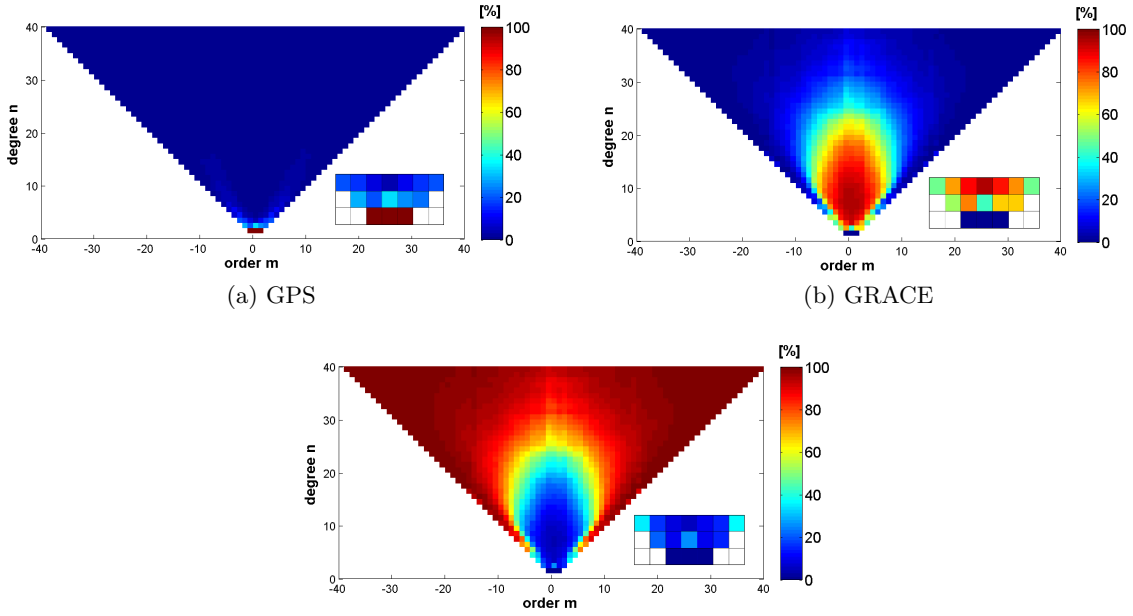

(a) GPS

(b) GRACE

(c) Regularization

Figure 23: Contribution of the input data to the estimated loading potential coefficients

4.2.4 GPSonly solution

As can be seen in Fig. 23, only GPS data contributes to degree-1 loading potential coefficients. This raises the question whether adding GRACE data to a combined least squares adjustment is necessary at all.
In Fig. 24, the geocenter motion calculated with GPS data only as well as the geocenter motion calculated with GPS and GRACE data are displayed. Although the GRACE data does not directly contribute to degree-1 loading potential coefficients, it helps precisely separating lower degrees and therefore the solution becomes more accurate. Above all, the values of the amplitude (see table 5) could be minimized.

Table 5: Annual amplitude and phase of calculated geocenter motion

Solution		**Annual Amplitude [mm]**	**Annual Phase [doy]**
Geocenter motion	x:	1.5 ($\pm$ 0.10)	34 ($\pm$ 4)
	y:	1.8 ($\pm$ 0.09)	312 ($\pm$ 3)
	z:	4.3 ($\pm$ 0.09)	45 ($\pm$ 1)
Geocenter motion (GPS only)	x:	2.7 ($\pm$ 0.12)	55 ($\pm$ 3)
	y:	3.9 ($\pm$ 0.10)	314 ($\pm$ 2)
	z:	7.9 ($\pm$ 0.10)	34 ($\pm$ 1)

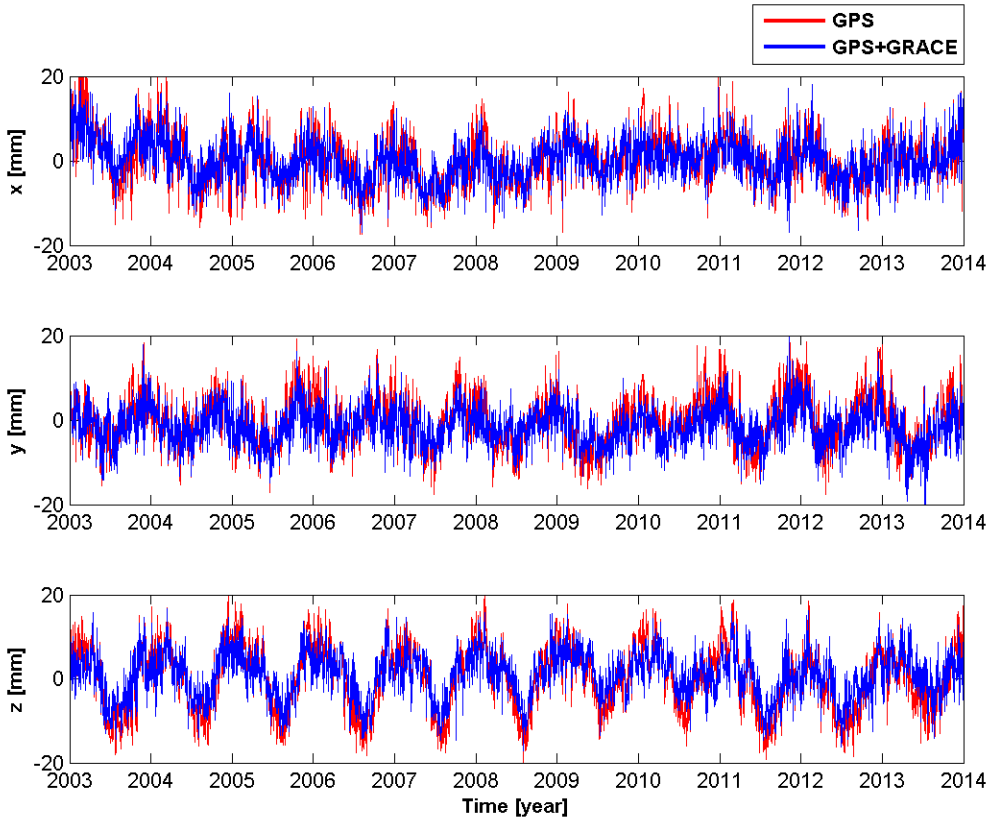

Figure 24: GPS only solution compared to the GPS+GRACE solution

4.2.5 Influences of the GPS accuracy specifications

For all calculations up to this point, standard deviations given by JPL were applied to the GPS observations before performing a variance component estimation together with GRACE and regularization data. Those standard deviations are for the lateral and longitudinal component in the order of a few sub-millimeters and for the radial component in the order of a few millimeters [JPL, 2014]. Because of different measurement accuracies, every observation has its own standard deviation and is therefore differently weighted in the least squares adjustment. The influence on the result by changing this a priori standard deviations has yet to be determined. To realize this, a standard deviation of $s = 3$ millimeters was applied to all observations. Consequently, all observations are equally weighted and the lateral as well as the longitudinal observations are assumed to be more inaccurate then declared by JPL.
In Fig. 25, the geocenter motion calculated with this standard deviation is displayed. The difference between this result and the one calculated with the standard deviations given by JPL can be seen in Fig. 26. Those variations are in the range of a few millimeters. When having a closer look at the amplitude and phase of those two time series in table 6, it can be seen that especially the phase of the x and y components as well as the amplitude of y and z show differences.

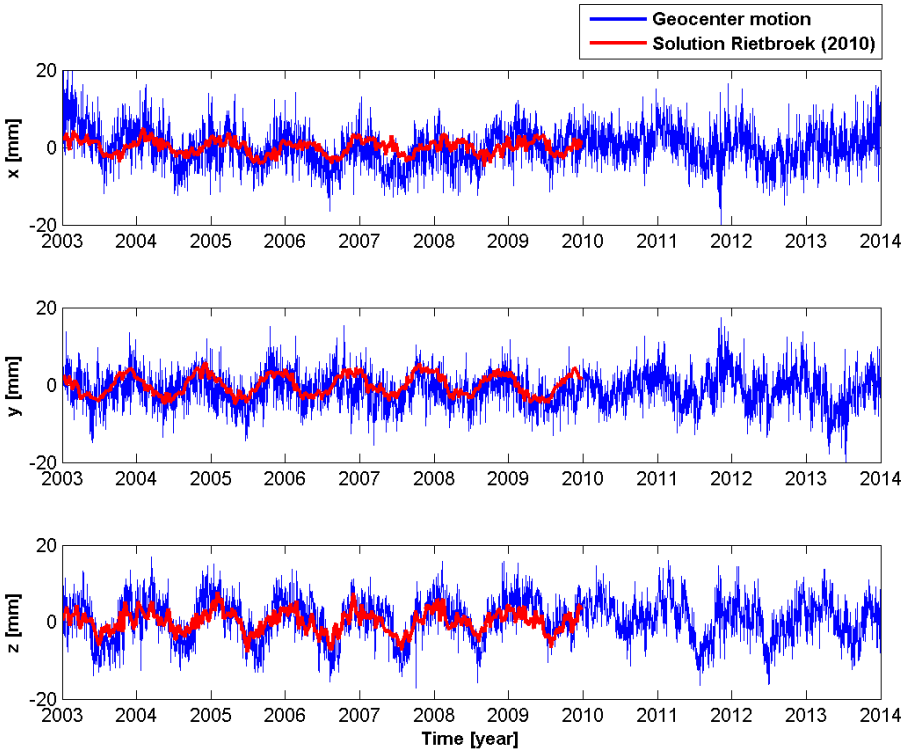

Figure 25: Geocenter motion calculated with a different standard deviation

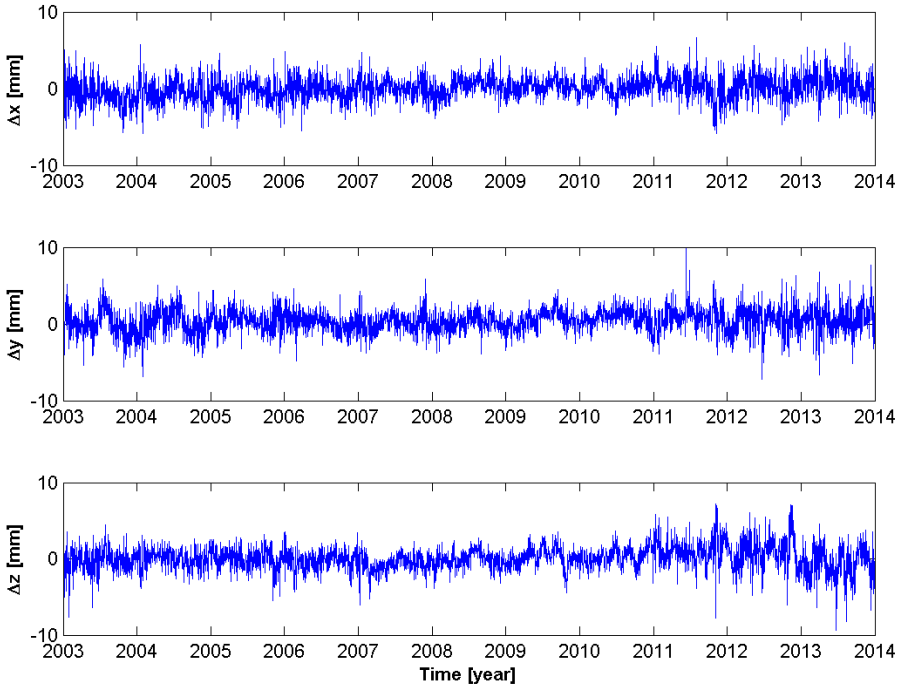

Figure 26: Difference of geocenter motions (new calculations - JPL data)

Table 6: Annual amplitude and phase of calculated geocenter motion

Solution		**Annual Amplitude [mm]**	**Annual Phase [doy]**
Geocenter motion	x:	1.5 ($\pm$ 0.10)	34 ($\pm$ 4)
	y:	1.8 ($\pm$ 0.09)	312 ($\pm$ 3)
	z:	4.3 ($\pm$ 0.09)	45 ($\pm$ 1)
Geocenter motion	x:	1.5 ($\pm$ 0.10)	44 ($\pm$ 4)
($s = 3\,mm$)	y:	1.5 ($\pm$ 0.09)	302 ($\pm$ 3)
	z:	4.1 ($\pm$ 0.09)	45 ($\pm$ 1)

In Fig. 27, the differences of the Helmert transformation parameters are displayed. It can be seen that a rotation as well as a small translation occur between the two solutions. This may appear due to the assumption that all observations (lateral, longitudinal and radial) have the same accuracy, which is not the fact when using the standard deviations given by JPL.
Additionally, a closer look was taken at the contributions of the input data to the estimated loading potential coefficients when equally weighting all GPS observations with a standard deviation of $s = 3\,mm$ (see Fig. 28). As discussed before, only the GPS input data is used to calculate degree-1 loading potential coefficients. However, compared to Fig. 23 it can be seen, that the GPS input data also mainly contributes to the degree-2 coefficients.
This current solution (using $s = 3\,mm$) was also computed with CM load Love numbers (cf. section 4.2.1). The differences between the CM and the CE solution are illustrated in Fig. 29 (for the geocenter motion) and in Fig. 30 (for the Helmert transformation parameters). Compared to the figures in section 4.2.1, the variations, especially in the geocenter motion, are much smaller.
Consequently, it seems that the result becomes more accurate when applying the same standard deviation of $s = 3\,mm$ to all GPS observations before performing the variance component estimation.

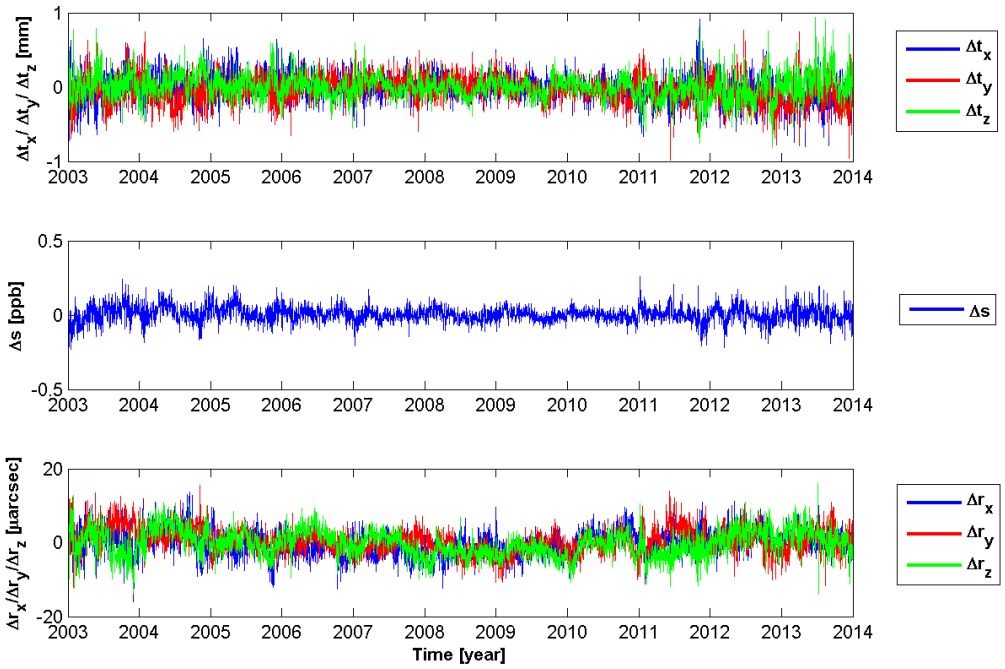

Figure 27: Differences of Helmert transformation paramters (new calculations - JPL data)

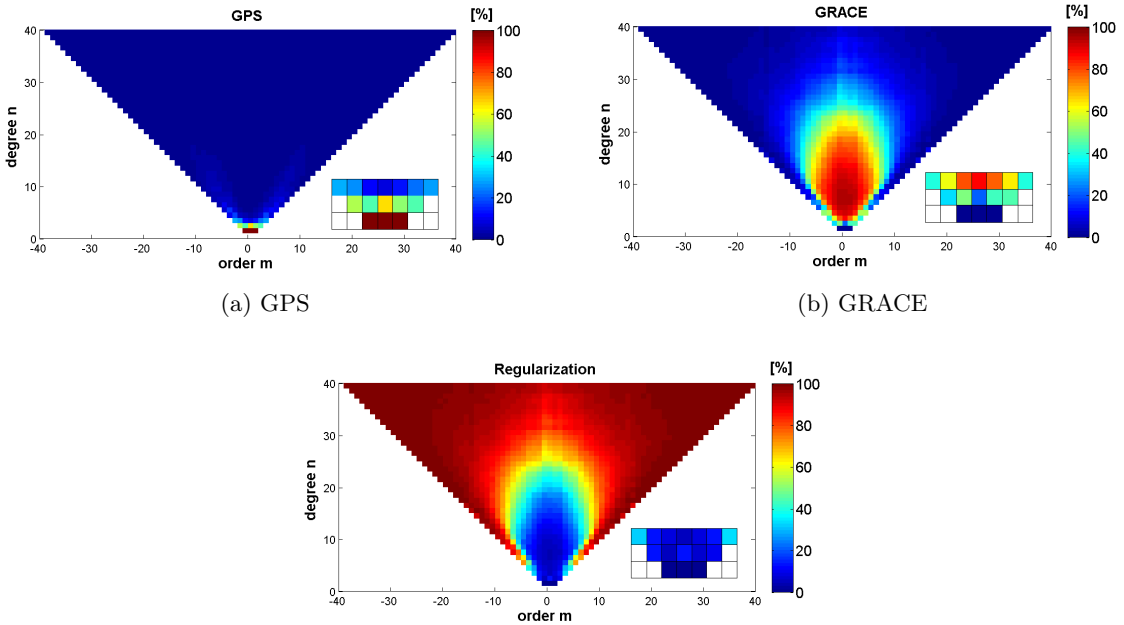

(a) GPS

(b) GRACE

(c) Regularization

Figure 28: Contribution of the input data to the estimated loading potential coefficients calculated with a different standard deviation

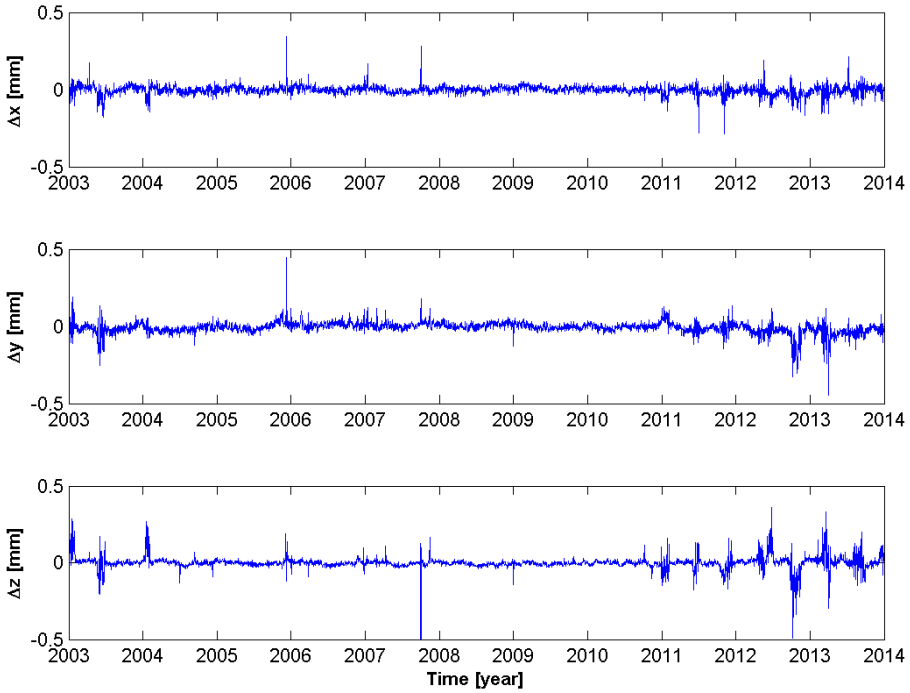

Figure 29: Difference of geocenter motions (CM-CE) calculated with a different std. deviation

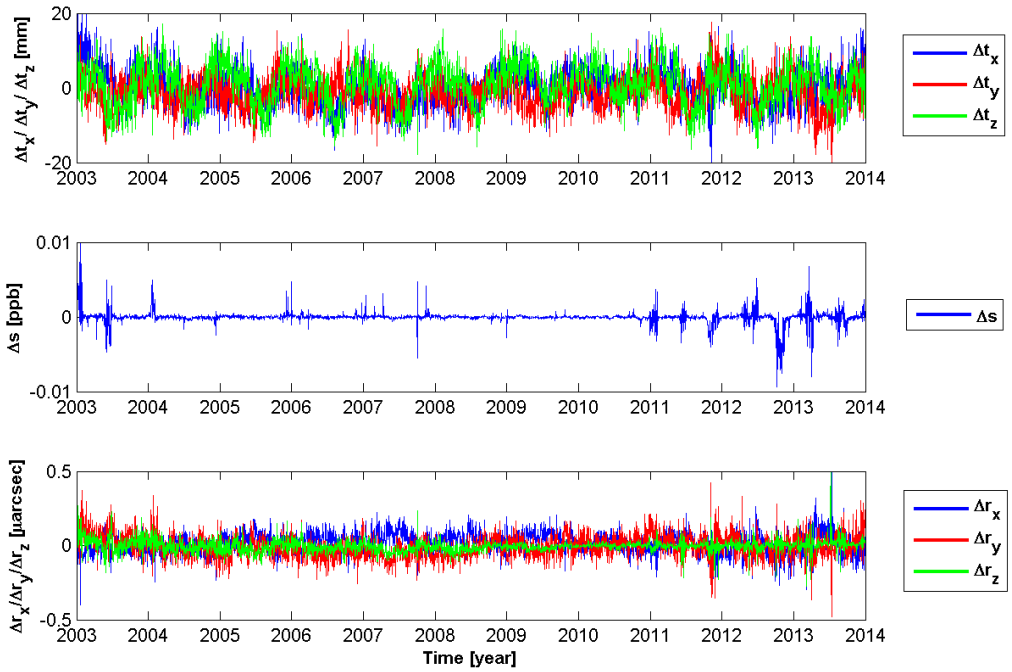

Figure 30: Difference of Helmert parameters (CM-CE) calculated with a different standard deviation

5 Conclusions and Outlook

As shown in this thesis, degree-1 load potential coefficients can be estimated with GPS deformation observations and subsequently the geocenter motion can be computed. When combining loading potential coefficients derived from GRACE observations with GPS observations in one least squares adjustment, the result becomes more accurate.
As GPS data is the most important input for the geocenter motion calculations, it is essential to pre-process this data as good as possible. First of all, jumps and the trend have to be eliminated from the GPS time series. Secondly, as the CN has to approximate the CE, the global distribution of GPS stations, of which data is used for calculations, has to be considered. Theoretically, stations have to be perfectly well distributed on the Earth's surface so that the CF ideally approximates the CE. In practice, using data of globally not well distributed stations does affect the result, however only minimally. This also affects the Helmert transformation parameters, which were estimated together with the loading potential coefficients and which represent deformation movements not caused by surface loading.
Furthermore, load Love numbers are also part of the equation to compute load potential coefficients. As the CE frame is suitable to model all dynamics of the solid Earth, CE load Love numbers were applied. However, when using CM load Love numbers instead, the result of the geocenter motion does not change. The only difference between those two solutions can be seen in the translation parameters (Helmert parameters). This can be explained by the fact that the CE and the CM only differ in one translation.
For further studies, it might be interesting to perform the calculations discussed in this thesis with different GPS input time series. More precisely, the influences of the input data's accuracy on the result could be analyzed in more detail. Moreover, the impact on the solution due to the number of stations available and their global distribution might be further investigated.

List of Figures

List of Tables

References

G. Blewitt. Self-consistency in reference frames, geocenter definition, and surface loading of the solid Earth. *JOURNAL OF GEOPHYSICAL RESEARCH*, 108(B2), 2003.

M. Cheng, B. Tapley, and J. Ries. Geocenter variations from analysis of SLR data. *International Association of Geodesy Symposia*, 2010.

W. E. Farrell. Deformation of the Earth by Surface Loads. *Reviews of geophysics and spacephysics*, 10(3):761–797, August 1972.

GFZ. GRACE payload, July 2014. URL `http://op.gfz-potsdam.de/grace/payload/payload.html`.

B. Hofmann-Wellenhof, H. Lichtenegger, and E. Wasle. *GNSS - Global Navigation Satellite Systems - GPS, GLONASS, Galileo & more*. SpringerWienNewYork, 2008.

IGS. International GNSS Service - tracking network, July 2014. URL `http://igs.org/`.

JPL. Jet Propulsion Laboratory - GPS time series, August 2014. URL `http://sideshow.jpl.nasa.gov/post/series.html`.

E. Kurtenbach. *Entwicklung eines Kalman-Filters zur Bestimmung kurzzeitiger Variationen des Erdschwerefeldes aus Daten der Satellitenmission GRACE*. PhD thesis, Universität Bonn, 2011.

T. Mayer-Gürr. GRACE gravity fields to mass changes. Geophysics and Geodynamics Script, TU Graz, 2012.

T. Mayer-Gürr, Norbert Zehentner, Beate Klinger, and Andreas Kvas. GRACE gravimetry, August 2014. URL `www.itsg.tugraz.at`.

H. Moritz and B. Hofmann-Wellenhof. *Physical Geodesy*. SpringerWienNewYork, 2006.

W. Niemeier. *Ausgleichungsrechnung*. de Gruyter, 2nd edition, 2008.

University of Texas. GRACE - gravity recovery and climate experiment, July 2014. URL `http://www.csr.utexas.edu/grace/`.

G. Prudent-Richard. Climate change impacts in the sub-antarctic islands. *Technical Report No 2 of ORNEC*, February 2009.

R. Rietbroek. *Retrieval of Sea Level and Surface Loading Variations from Geodetic Observations and Model Simulations: an Integrated Approach*. PhD thesis, Universität Bonn, January 2014.

R. Rietbroek, M. Fritsche, S.-E. Brunnabend, I. Daras, J. Kusche, J. Schröter, F. Flechtner, and R. Dietrich. Global surface mass from a new combination of GRACE, modelled OBP and reprocessed GPS data. *Journal of Geodynamics*, (59-60):64–71, 2012.

G. Spada. ALMA, a Fortran program for computing the viscoelastic Love numbers of a spherically symmetric planet. *Computers & Geosciences*, 34:667–687, June 2008.

S. Swenson and J. Wahr. Estimating geocenter variations from a combination of GRACE and ocean model output. *Journal of Geophysical Research*, August 2008.

B. D. Tapley, S. Bettadpur, M. Watkins, and C. Reigber. The gravity recovery and climate experiment: Mission overview and early results. *Geophysical Resesarch Letters*, 31(9), May 2004.

X. Wu, J. Rayb, and T. van Damc. Geocenter motion and its geodetic and geophysical implications. *Journal of Geodynamics*, 58:44–61, July 2012.

ZAMG. Unwetterbericht für 2009, August 2014. URL `http://www.zamg.ac.at/`.